Biogeosciences Discuss., 10, 8637–8683, 2013
www.biogeosciences-discuss.net/10/8637/2013/
doi:10.5194/bgd-10-8637-2013

Biogeosciences Discussions
Open Access

Dynamic seasonal nitrogen cycling in response to anthropogenic N-loading in a tropical catchment, Athi–Galana–Sabaki River, Kenya

T. R. Marwick[1], F. Tamooh[1,2], B. Ogwoka[2], C. Teodoru[1], A. V. Borges[3], F. Darchambeau[3], and S. Bouillon[1]

[1]Katholieke Universiteit Leuven (KU Leuven), Department of Earth and Environmental Sciences, Celestijnenlaan 200E, 3001 Leuven, Belgium
[2]Kenya Wildlife Service, P.O. Box 82144–80100, Mombasa, Kenya
[3]Unité d'Océanographie Chimique, Université de Liège (ULg), Belgium

Received: 19 April 2013 – Accepted: 4 May 2013 – Published: 23 May 2013

Correspondence to: T. R. Marwick (trentrichard.marwick@ees.kuleuven.be)

Published by Copernicus Publications on behalf of the European Geosciences Union.

Abstract

As part of a broader study on the riverine biogeochemistry in the Athi–Galana–Sabaki (A–G–S) River catchment (Kenya), we present data constraining the sources, transit and transformation of multiple nitrogen (N) species as they flow through the A–G–S catchment ($\sim 47\,000\,km^2$). The data-set was obtained in August–September 2011, November 2011, and April–May 2012, covering the dry season, short-rain season and long-rain season respectively. Release of, largely untreated, waste water from the city of Nairobi had a profound impact on the biogeochemistry of the upper Athi river, leading to low dissolved oxygen (DO) saturation levels (67–36 %), high ammonium (NH_4^+) concentrations (1193–123 $\mu mol\,L^{-1}$), and high dissolved methane (CH_4) concentrations (6729–3765 $nmol\,L^{-1}$). Total dissolved inorganic nitrogen (DIN) concentrations entering the study area were highest during the dry season (1195 $\mu mol\,L^{-1}$), while total DIN concentration was an order of magnitude lower during the short and long rain seasons (212 and 193 $\mu mol\,L^{-1}$, respectively). During the rain seasons, low water residence time led to relatively minimal instream N-cycling prior to discharge to the ocean. Conversely, increased residence time during the dry season creates two differences comparative to wet season conditions, where (1) intense cycling and removal of DIN in the upper- to mid-catchment leads to significantly less DIN export during the dry season, and (2) as a result of the intense DIN cycling, dry season particulate N export is significantly enriched in the N stable isotope ratio ($\delta^{15}N_{PN}$), strongly reflecting the dominance of organic matter as the prevailing source of riverine nitrogen. The rapid removal of NH_4^+ in the upper study area during the dry season was accompanied by a quantitatively similar production of NO_3^- and nitrous oxide (N_2O) downstream, pointing towards strong nitrification over this reach during the dry season. Nitrous oxide produced was rapidly degassed downstream, while the elevated NO_3^- concentrations steadily decreased to levels observed elsewhere in more pristine African river networks. Low pelagic primary production rates over the same reach suggest that benthic denitrification was the dominant process controlling the removal of NO_3^-, although large cyanobacterial blooms

BGD
10, 8637–8683, 2013

further downstream highlight the significant role of DIN assimilation by primary producers in the drainage network. The intense upper- to mid-catchment N-cycling leads to a significantly enriched $\delta^{15}N_{PN}$ during the dry season (mean: +16.5 ± 8.2‰ but reaching as high as +31.5‰) compared to the short (+7.3 ± 2.6‰) and long (+7.6 ± 5.9‰) rain seasons. A strong correlation found between seasonal $\delta^{15}N_{PN}$ and oxygen stable isotope ratios ($\delta^{18}O_{H_2O}$; as a proxy of freshwater discharge) presents the possibility of employing a combination of proxies, such as $\delta^{15}N_{PN}$ of sediments, bivalves and near-shore corals, to reconstruct how historical land-use changes have influenced nitrogen cycling within the catchment, whilst potentially providing foresight in the impacts of future land management decisions.

1 Introduction

Human activities over the last two centuries have drastically influenced regional and global nitrogen (N) cycles (Galloway et al., 1995; Howarth et al., 1996; Galloway and Cowling, 2002). Prior to the industrial revolution, the dominant processes fixing atmospheric dinitrogen (N_2) to reactive (biologically available) N included lightning, bacterial nitrogen fixation (BNF) and volcanic activity, while return of N_2 gases to the atmosphere through denitrification and the annamox pathway closed the global N cycle (Ayres et al., 1994; Canfield et al., 2010). Post-industrial revolution, and related to rising global populations, the Haber–Bosch process (and associated fertiliser application and industrial usage), fossil fuel combustion, and increased cultivation of BNF crops currently account for about 45 % of total annual fixed N produced globally (Canfield et al., 2010). Much of this reactive N enters streams and rivers (Green et al., 2004; Seitzinger et al., 2006) through point sources (predominantly urban and industrial effluents) or diffusive sources (such as leaching from agricultural land and atmospheric deposition) (Bouwman et al., 2005) with severe environmental implications downstream, including eutrophication, acidification of water bodies, fish kills, loss of biodiversity (Vitousek et al., 1997; Carpenter et al., 1998), and the emission to the atmosphere of nitrous

BGD
10, 8637–8683, 2013

oxide (N_2O) (Seitzinger and Kroeze, 1998) a potent greenhouse gas (with a global warming potential ~ 300 times greater than carbon dioxide (CO_2)) and the dominant ozone-depleting substance in the 21st century (Ravishankara et al., 2009).

The dominant forms of reactive N (i.e. dissolved inorganic nitrogen, DIN) entering freshwaters are ammonium (NH_4^+) and nitrate (NO_3^-), albeit in low concentrations unless inputs are linked to N-saturated forests, grasslands, agroecosystems, or suburban landscapes (Galloway et al., 2003). A multitude of interrelated microbial metabolic pathways and abiotic reactions are involved in the transformation and removal of N from aquatic systems, including N_2 fixation, ammonification, anaerobic NH_4^+ oxidation (anammox), nitrification, denitrification, dissimilatory reduction of NO_3^- to NH_4^+ (DNRA), assimilation of DIN into biomass, NH_3 volatilization, and NH_4^+ adsorption and desorption. These pathways may be (chemo)autotrophic or heterotrophic, with the prevailing pathway dependant on the presence or absence of oxygen and organic carbon (OC) within the local environment (Trimmer et al., 2012). Resource stoichiometry (OC : NO_3^-) may also control NO_3^- accumulation and transformation within a system through the regulation of various microbial processes linking the N cycle with carbon cycling (Taylor and Townsend, 2010). Other important controls on the quantity of DIN removed at the reach scale are water residence time and the NO_3^- load per unit area of sediment (Galloway et al., 2003; Trimmer et al., 2012). Under high flow conditions (and/or high N-loading) there may be comparatively minimal turnover of total NO_3^- load at the reach scale (Trimmer et al., 2012), whereas an extended water residence time provides greater opportunity for contact between DIN in the water column and (oxic) surface and (anoxic) hyporheic sediments. Also, under situations of high organic matter decomposition or strongly enhanced primary production and respiration, inhibition of nitrification may occur due to the development of hypoxic, or anoxic, conditions in the water column, and consequently inhibits denitrification due to the decreased production of NH_4^+.

Despite the low residence time of fluvial transported materials within the aquatic system relative to their terrestrial residence times, rivers can efficiently remove DIN, often denitrifying as much as 30 % to 70 % of external N-inputs (Galloway et al., 2003).

BGD
10, 8637–8683, 2013

Lakes and reservoirs are two features which extend water residence time within a river network, thereby enhancing particle settling and nutrient processing through which N removal may proceed by sedimentation and/or denitrification processes (Wetzel, 2001). Recent modeling of lentic systems has conservatively estimated their ability to remove 19.7 $Tg\,N\,yr^{-1}$ from watersheds globally (Harrison et al., 2009), with small lakes (< 50 km^2) accounting for almost half the global total removal and reservoirs approximately 33 %. Clearly, this ability of upstream lakes and reservoirs to significantly remove N from river systems can effectively alleviate downstream eutrophication and hypoxia, for example.

Within the oxygenated zone of the water column, chemo-autotrophic bacteria (e.g. *Nitrosomonas* sp., *Nitrosococcus* sp.) and archaea (*Nitrosopumilus*, *Nitrosotalea*, *Nitrosocaldus*, Cao et al., 2013) oxidise NH_4^+ to nitrite (NO_2^-), with the NO_2^- subsequently oxidised to NO_3^- by an alternate group of bacteria (*Nitrobacter* sp.), completing the nitrification pathway. The relative importance of archaea and bacteria in NH_4^+ oxidation, and the related environmental drivers are still poorly constrained, in particular in freshwater environments (French et al., 2012; Mylène et al., 2013). Removal from the system through production and efflux of N_2 gas to the atmosphere may occur through denitrification, but of greater concern is the production and efflux of N_2O, an effective greenhouse gas (with a global warming potential ~ 300 times greater than CO_2) that also breaks down stratospheric ozone. The production of N_2O is bypassed through the anammox pathway, a two-step process by which NH_4^+ is initially converted to the intermediate N_2H_4 and finally N_2 gas (Canfield et al., 2010). Denitrification, another anaerobic pathway operating in anoxic zones, reduces the NO_3^- produced during nitrification to either N_2O or N_2 gases. N_2O can also be produced as a by-product during nitrification, although, denitrification is assumed to be the dominant process producing N_2O in temperate freshwaters (Beaulieu et al., 2011). Ammonia oxidizers can also produce N_2O through nitrifier denitrification (Wrage et al., 2001). With the growing appreciation of the effects of elevated N_2O in the atmosphere comes the necessity to better constrain the impacts of increased N-loading of aquatic systems.

BGD
10, 8637–8683, 2013

The application of N stable isotope ratios (δ^{15}N) is a valuable tool to delineate sources of N in aquatic systems (Risk et al., 2009). This approach is based on the preferential involvement of the isotopically lighter ^{14}N, relative to the heavier ^{15}N, in various biogeochemical reactions, resulting in isotopic fractionation of the residual N pool and subsequent changes to the ^{15}N : ^{14}N ratio (Owens, 1987). Dominant N sources to aquatic systems often have distinguishable δ^{15}N signatures. The biological fixation of atmospheric N (δ^{15}N = 0‰) generally results in minimal fractionation of ^{15}N (0‰ to +2‰), while the production of artificial fertilizer produces δ^{15}N from −2‰ to +4‰ (Vitoria et al., 2004). N in organic waste inputs is characterised by enriched δ^{15}N values, with NO_3^- from wastewater, sewage and manure displaying δ^{15}N values of +8‰ to +22‰ (Aravena et al., 1993; Widory et al., 2005). Recent studies have employed this technique to trace the movement of sewage-derived N within aquatic ecosystems (e.g. Costanzo et al., 2001; De Brabandere et al., 2002; Lapointe et al., 2005; Risk et al., 2009; Moynihan et al., 2012). Elliot and Brush (2006) correlated a +2‰ to +7‰ change in δ^{15}N of a wetland sedimented organic matter core spanning 350 yr to a shift in land use from forested conditions to increased nutrient inputs from human waste, highlighting the potential of this technique to expand our temporal frame for assessing land use change on catchment N cycling.

To date, the largest effects of increased reactive N inputs have occurred in developed countries of the Temperate Zone, largely driven by synthetic fertiliser application (Holland et al., 1999; Howarth, 2008). Yet, rapidly increasing populations in developing countries of the tropics are leading to increased ecosystem N-loading within these regions. The consequences of increased N-loading to global river catchments, and specifically the tropics, are already being observed and forecasted (Caraco and Cole, 1999; Downing et al., 1999; Bouwman et al., 2005; Seitzinger et al., 2010). Recent modelling of DIN export to coastal waters of 524 African river catchments has estimated a 35 % increase in yield from 1970 to 2000, with two thirds of total yield entering the oceans in the 0–35° S latitude band (Yasin et al., 2010). A further 4–47 % increase in total river export of DIN is modelled for the period 2000–2050, with the quantity of

BGD
10, 8637–8683, 2013

anthropogenically-influenced N fixation greater than natural (pre-industrial) N_2 fixation rates.

Through draining Nairobi, Kenya, the Athi–Galana–Sabaki (A–G–S) catchment provides an example of human-induced N-loading within inland water systems of tropical Africa. Following British settlement and the establishment of Nairobi in 1899, the urban population expanded from 11 500 in 1906 (Olima, 2001) to over 3.1 million by 2009 (K.N.B.S., 2009), with approximately half the current population living in slums lacking adequate sewage and sanitation services (Dafe, 2009). Many of the informal settlements of Nairobi are positioned within the riparian fringe of the A–G–S headwaters (Kithiia, 2012), with raw sewage directly discharged to the streams. Poor waste disposal and management strategies have led to increasing water quality degradation (Kitthia and Wambua, 2010), where, for example, the total quantity of water passing through the A–G–S headwater streams ($36.7 \times 10^6\,m^3\,yr^{-1}$) and into the main channel equates to less than the combined domestic and industrial waste discharge for the region (Kitthia, 2012).

Previous research has revealed substantial changes in the A–G–S catchment over the past decennia. Based on geochemical data recorded in corals near the Sabaki River mouth, Fleitmann et al. (2007) suggested a stable riverine sediment flux at the outlet between 1700 and 1900, but a 5- to 10-fold increase in sediment delivery up to the period 1974–1980. This increasing sediment flux has been attributed to expansion of intensive agricultural practises in the headwaters of the catchment, unregulated land use, deforestation, and severe droughts in the 1970's. Yet, little is known of the temporal and spatial processes controlling the transport and cycling of N through the A–G–S network.

As part of a broader study on the riverine biogeochemistry in the A–G–S catchment, we present data collected during three climatic seasons and a one year bi-weekly sampling regime to constrain the sources, transformations and transit of multiple N species as they flow through the A–G–S catchment, stretching from downstream of urban Nairobi to the outlet at the Indian Ocean.

BGD
10, 8637–8683, 2013

2 Materials and methods

2.1 Study area

Athi–Galana–Sabaki (A–G–S) is the second largest river catchment in Kenya draining a total catchment area of 46 600 km^2. A–G–S River catchment has its headwaters situated in central and south-east Kenya (Fig. 1). Upstream of Nairobi, the headwaters forming the Nairobi River initially drain agricultural (predominantly tea and coffee plantations) systems which provide the livelihood of 70 % of the regional population (Kitthia, 1997). Since 1920 the total land area of Kenya dedicated to tea and coffee cultivation increased by 98 % and 67 %, respectively (Kitheka et al., 2004). Most of this area, including the upper A–G–S catchment, is located in the high rainfall highlands of central Kenya and was previously forested (Kitheka et al., 2004). The sub-catchment around Nairobi city is dominated by industrial activities and informal settlements, with subsequent livestock and small-scale irrigation activities downstream prior to the Nairobi River joining the main Athi River at 1440 m a.s.l. and 590 km upstream of the outlet. The combination of these land-uses and climatic variability within the region have resulted in severe soil erosion and increased sediment transport from the headwaters (Kitthia, 1997; Kitheka et al., 2004; Fleitmann et al., 2007). Downstream of the confluence with the Nairobi River, the Athi follows a confined channel along the southern edge of the Yatta Plateau between Thika and the confluence of the Tsavo River (at 240 m a.s.l.), the only major perennial tributary, which drains the northern slopes of Mount Kilimanjaro. Ephemeral tributaries emanate from Amboseli, Chyulu Hills and Taita Hills in the mid-catchment. Severe soil erosion in the mid-catchment, particularly within the agricultural Machakos district, dates back to the 1930s (Tiffen et al., 1994), being previously linked to destruction of vegetation for charcoal burning, poor cultivation methods and over-grazing (Ongwenyi et al., 1993). Following the confluence of the Athi with the Tsavo, the river becomes known as the Galana, opening out into a broader floodplain with a meandering habit (Oosterom, 1988). The Galana follows this habit for 220 km through semi-arid savannah plains before emptying into the West

BGD
10, 8637–8683, 2013

Indian Ocean near the Malindi–Watamu reef complex as the Sabaki River. Seawater incursion is impeded in the lower reaches of the Sabaki as a result of a relatively steep gradient ($3 \times 10^{-4}\,\mathrm{m\,m^{-1}}$).

Annual precipitation ranges between 800–1200 $\mathrm{mm\,yr^{-1}}$ in the highly populated central highlands, to 400–800 $\mathrm{mm\,yr^{-1}}$ in the less populated semi-arid south-east. Two dry seasons are interspersed annually by a short (October–December, OND) and long (March–May, MAM) rain season. Accordingly, the annual hydrograph experiences bimodal discharge, with seasonal variation between 0.5 $\mathrm{m^3\,s^{-1}}$ and 758 $\mathrm{m^3\,s^{-1}}$ (1957–1979 mean: 48.8 $\mathrm{m^3\,s^{-1}}$) (Fleitmann et al., 2007). More recent discharge data from 2001–2004 places the mean discharge of the A–G–S outlet at 73.0 $\mathrm{m^3\,s^{-1}}$ (Kitheka et al., 2004). Mean annual flow of the perennial Tsavo River has increased from 4 $\mathrm{m^3\,s^{-1}}$ to 10 $\mathrm{m^3\,s^{-1}}$ between the 1950s and present conditions, attributed to the increased melting of glaciers on Mount Kilimanjaro (Kitheka et al., 2004). Oscillations between El Niño and La Niña conditions within Kenya have a strong influence on the decadal patterns of river discharge, where extended severe drought can be broken by intense and destructive flooding (Mogaka et al., 2006). No reservoirs have yet been developed within the catchment for the harnessing of hydropower (Kitheka et al., 2004), although a number of small abandoned dams, originally for industrial water abstraction purposes, are present on the Nairobi headwaters (e.g. Nairobi dam). The combination of changing land-use practises, highly variable climatic conditions and highly erosive native soils has led to modern sediment flux estimates between 7.5 and 14.3 million $\mathrm{t\,yr^{-1}}$ (Van Katwijk et al., 1993), equating to a soil erosion rate of 110–210 $\mathrm{t\,km^{-2}\,yr^{-1}}$. Dunne (1979) estimated that 80 % of the annual mean sediment yield can be carried by the upper 10 % of daily flows.

2.2 Sampling and analytical techniques

Sampling was conducted at 20–25 sites throughout the A–G–S catchment at the end of the long dry season (August–September 2011), and during the short rain (November 2011; OND rains) and long rain seasons (April 2012; MAM rains). Headwater regions

BGD
10, 8637–8683, 2013

above and within Nairobi were ignored due to the overriding influence of pollutants on stream quality. Fourteen Falls, 23 km downstream of the Athi–Nairobi confluence, was selected as the most upstream sampling site, with 14 sites following at approximately 40 km intervals leading to the outlet. The most downstream site, positioned 5 km upstream of the river mouth, was also equipped to sample fortnightly, commencing August 2011. The sole contributing sub-catchment sampled during the dry season was the Tsavo, whereas during both the OND and MAM rains it was possible to sample within the Keite and Muoni watersheds also.

In-situ physico-chemical parameters, including water temperature, dissolved oxygen (DO) content, pH and (in-situ and specific) conductivity, were measured using a combination of a YSI Professional Plus (Pro Plus, Quattro cable bulkhead) and YSI Professional Optical Dissolved Oxygen (Pro ODO) instrument. Calibrations for pH were performed daily using National Bureau of Standards (NBS) buffers of pH 4 and 7.

Water samples for nutrient analysis (NH_4^+ and NO_3^-) were obtained in 20 mL scintillation vials by pre-filtering surface water through pre-combusted GF/F filters (0.7 µm), with further filtration through 0.2 µm syringe filters and preserved with 20 µL of saturated $HgCl_2$. Samples for analysis of $\delta^{15}N_{PN}$ were obtained by filtering a known volume of surface water on pre-combusted (overnight at 450 °C) 47 mm GF/F filters (0.7 µm). Filters were dried and a section from each filter packed into Ag cups for $\delta^{15}N_{PN}$ analysis. Samples for particulate organic carbon (POC), particulate N (PN), and $\delta^{13}C_{POC}$ were obtained in the same manner as $\delta^{15}N_{PN}$ samples, though filtered through a pre-combusted (500 °C for 4 h) 25 mm GF/F filter (nominal porosity = 0.7 µm) which was air-dried on-site. These filters were later exposed to HCl fumes for 4 h to remove inorganic C, re-dried and packed in Ag cups.

A Niskin bottle was used to collect surface water for dissolved methane (CH_4) and N_2O samples. Samples were stored in 60 mL glass serum vials, poisoned with 20 µL $HgCl_2$, closed air-tight with butyl stopper, and sealed with an aluminium cap. Remaining water from the Niskin bottle was used for measuring community respiration rates. Between 5–7 60 mL borosilicate biological oxygen demand bottles with stoppers

BGD
10, 8637–8683, 2013

(Wheaton) were over-filled, sealed and stored in an isothermal insulated box. After approximately 24 h, DO ($mg\,L^{-1}$) was measured and used to calculate an average community respiration rate (R):

$$R = \frac{DO_r - DO_i}{t_e - t_i} \quad (1)$$

where DO_r is the in-situ DO ($mg\,L^{-1}$) of the river water, DO_i the DO ($mg\,L^{-1}$) following incubation, and t_i and t_e the initial and end time of the incubation. During the dry season campaign, DO_r was assumed from the in-stream measurements of the YSI Pro-ODO instrument, whereas during the OND and MAM rain campaigns three extra incubation bottles were filled and the DO ($mg\,L^{-1}$) immediately measured using the YSI Pro-ODO instrument, with the average of the three bottles used as DO_r.

Water samples for Total Alkalinity (TA) were obtained by prefiltering surface water through pre-combusted GF/F filters (0.7 µm), with further filtration through 0.2 µm syringe filters in high-density polyethylene bottles. TA was analyzed by automated electrotitration on 50 mL samples with 0.1 $mol\,L^{-1}$ HCl as titrant (reproducibility estimated as better than ±3 $\mu mol\,kg^{-1}$ based on replicate analyses).

In-situ pelagic primary production measurements were performed by filling two 500 mL polycarbonate bottles with surface water and adding 500 µL of a ^{13}C-spike solution (> 99.8 % $\delta^{13}C$ $NaH^{13}CO_3$, ±40 mg dissolved in 12 mL of 0.2 µm filtered surface water). Bottles were incubated in-stream under ambient light and temperature conditions for approximately 2 h, after which a subsample from each bottle was filtered onto separate pre-combusted (500 °C for 4 h) 25 mm GF/F filter (nominal porosity = 0.7 µm) and air-dried on-site. These filters were later exposed to HCl fumes for 4 h to remove inorganic C, re-dried and packed in Ag cups. A separate 12 mL glass headspace vial, for measurement of the ^{13}C-DIC enrichment ($\delta^{13}C_{DIC-PP}$), was also filled from each bottle with the addition of 10 µL $HgCl_2$ to inhibit further biological activity.

Analysis of primary production filters and the $\delta^{13}C_{DIC-PP}$ followed the procedures outlined below for POC and $\delta^{13}C_{DIC}$, respectively. Primary production rates (PP) were

BGD
10, 8637–8683, 2013

calculated based on Hama et al. (1983):

$$PP = \frac{POC_f(\%^{13}POC_f - \%^{13}POC_i)}{t(\%^{13}DIC - \%^{13}POC_i)} \quad (2)$$

where t is the incubation time, $\%^{13}DIC$ the percentage ^{13}C of the DIC after the bottles had been spiked, POC_f the particulate organic carbon after incubation, and $\%^{13}POC_i$ and $\%^{13}POC_f$ the initial and final (i.e. after incubation) percentage ^{13}C of the POC, respectively. Where the difference between $\%^{13}POC_i$ and $\%^{13}POC_f$ was < 1‰, PP was considered below detection limits (< d.l.) at these sites.

Laboratory analysis of NH_4^+ (based on the modified Berthelot reaction) and NO_3^- (based on the hydrazanium sulfate reduction method) was conducted on a 5 mL subsample of the field sample, and measured on a Skalar Continuous Flow Analyser (model 5100) with FlowAccess V3 software.

POC, PN, $\delta^{13}C_{POC}$ and $\delta^{15}N_{PN}$ were determined on a Thermo elemental analyzer-isotope ratio mass spectrometer (EA-IRMS) system (FlashHT with DeltaV Advantage), using the thermal conductivity detector (TCD) signal of the EA to quantify PN, and by monitoring either the m/z 28 and 29, or m/z 44, 45, and 46 signal on the IRMS. Calibration of $\delta^{15}N_{PN}$ was performed with IAEA-N1, while IAEA-C6 and acetanilide were used for $\delta^{13}C_{POC}$, with all standards internally calibrated against international standards. Reproducibility of $\delta^{15}N_{PN}$ and $\delta^{13}C_{POC}$ measurements was typically better than ±0.2‰, while relative standard deviations for calibration standards for POC and PN measurements were typically < 2% and always < 5%. POC : PN ratios are presented on a weight : weight basis.

Concentrations of CH_4 and N_2O were determined by a head-space equilibration technique (20 mL N_2 headspace in 60 mL serum bottles) and measured by gas chromatography (GC; Weiss, 1981) with flame ionization detection (FID) and electron capture detection (ECD). The SRI 8610C GC-FID-ECD was calibrated with $CH_4 : CO_2 : N_2O : N_2$ mixtures (Air Liquide Belgium) of 1, 10 and 30 ppm CH_4 and of 0.2, 2.0 and

BGD
10, 8637–8683, 2013

6.0 ppm N_2O, and using the solubility coefficients of Yamamoto et al. (1976) for CH_4 and Weiss and Price (1980) for N_2O.

$\delta^{18}O_{H_2O}$ analyses were conducted as described by Gillikin and Bouillon (2007). 0.5 mL of sampled water (from the bulk 20 mL nutrient sample) was added to a 12 mL glass headspace vial and subsequently flushed with He, followed by the addition of 0.25 mL of pure CO_2 gas using a gas-tight syringe. Following overnight equilibration, approximately 1 mL of the headspace was injected into the abovementioned EA-IRMS configuration. Three internal working standards covering a range of $\delta^{18}O$ values between −22.3 and +6.9‰, calibrated versus SMOW (Vienna Standard Mean Ocean Water; 0‰), GISP (Greenland Ice Sheet Precipitation; −24.76‰) and SLAP (Standard Light Antarctic Precipitation; −55.50‰) were used to calibrate sample $\delta^{18}O_{H_2O}$ data.

3 Results

Water temperature along the main channel increased downstream during all campaigns (Fig. 2a). In-situ pH was significantly higher during the dry season compared to both the OND (paired *t* test (PTT), $p =< 0.001$, $n = 20$) and MAM rainy seasons (PTT, $p =< 0.001$, $n = 19$), especially in the lower reaches of the main channel, whilst also significantly lower (PTT, $p = 0.01$, $n = 23$) during the MAM rains comparative to OND rains (Fig. 2b). DO saturation levels ranged between 36.1–154.2 %, 56.0–108.1 % and 66.8–111.0 % during the dry season, OND and MAM rains respectively, with surface waters nearing hypoxic conditions (DO saturation level < 30 %) at S1 (36.1 % DO) and S2 (37.2 %) during the dry season (Fig. 2c). DO was significantly higher (PTT, $p = 0.07$, $n = 20$) during the dry season than during the OND rains, which were also significantly lower (PTT, $p = 0.05$, $n = 23$) than the MAM rains.

Total DIN concentrations at S1 were highest during the dry season (1195 µmol L^{-1}), almost completely in the form of NH_4^+ (99.8 %). Total DIN was considerably lower at S1 during the OND (430 µmol L^{-1}) and MAM (222 µmol L^{-1}) rains, with NH_4^+ still the

BGD
10, 8637–8683, 2013

dominant DIN form entering the study area (72.0 % and 55.4 %, respectively). Total DIN in the Tsavo River at S12 (9 km upstream from the Tsavo–Athi confluence, the single perennial tributary measured within the study area) displayed less variability (dry season: 56.5 $\mu mol\,L^{-1}$; OND: 56.4 $\mu mol\,L^{-1}$; MAM: 88.3 $\mu mol\,L^{-1}$), and was dominated by NO_3^- across all seasons (dry season: 66.8 % of total DIN; OND: 97.0 %; MAM: 62.6 %).

NH_4^+ decreased one to two orders of magnitudes from S1 to the outlet over all seasons (Fig. 3a). Concentrations ranged from 13.8–1192.9 $\mu mol\,L^{-1}$ (mean: 84.3 ± 263.5 $\mu mol\,L^{-1}$), 0.4–309.7 $\mu mol\,L^{-1}$ (18.5 ± 61.2 $\mu mol\,L^{-1}$), and 8.4–123.0 $\mu mol\,L^{-1}$ (24.2 ± 25.7 $\mu mol\,L^{-1}$) during the dry, OND and MAM rain season, respectively. NH_4^+ concentrations during the OND rains were significantly higher than during the dry season (Wilcoxon signed rank test (WSRT), $p =< 0.001$, $n = 20$) and MAM rains (WRST, $p = 0.004$, $n = 22$). NO_3^- concentrations ranged between 0.2–857.6 $\mu mol\,L^{-1}$ (dry season mean: 195.7 ± 309.4 $\mu mol\,L^{-1}$), 40.3–537.6 $\mu mol\,L^{-1}$ (OND rain mean: 188.5 ± 145.4 $\mu mol\,L^{-1}$), and 24.0–398.8 $\mu mol\,L^{-1}$ (MAM rain mean: 127.7 ± 95.5 $\mu mol\,L^{-1}$) (Fig. 3b). When sites are split above and below 450 m a.s.l., NO_3^- concentrations < 450 m a.s.l. in the dry season are significantly lower than during both the OND (PTT, $p =< 0.001$, $n = 8$) and MAM rains (PTT, $p = 0.002$, $n = 6$). The rapid decrease of NH_4^+ between S1 and S2 is accompanied by an increase of NO_3^- over the same stretch during all seasons, though being most pronounced in the dry season. Like NO_3^-, dissolved N_2O peaked at S2 (196 $nmol\,L^{-1}$) during the dry season, decreasing rapidly by S3 (18 $nmol\,L^{-1}$) (Fig. 4a). Dissolved N_2O generally decreased downstream over all seasons, with significantly higher concentrations (WSRT, $p = 0.019$, $n = 22$) during the OND rains compared to the MAM rains.

$\delta^{15}N_{PN}$ displayed marked differences between the dry and rain seasons, with heavily enriched signatures at most sites during the dry season (Fig. 5). $\delta^{15}N_{PN}$ signatures during the dry season (range: +3.1 to +31.5 ‰; mean: +16.5 ± 8.2 ‰) were significantly enriched compared to both OND (range: −1.1 to +13.6 ‰; mean: +7.3 ± 2.6 ‰; PTT, $p =< 0.001$, $n = 19$) and MAM (range: 0.0 to +19.8 ‰; mean: +7.6 ± 5.9 ‰; PTT,

BGD
10, 8637–8683, 2013

$p = 0.002$, $n = 19$) signatures. $\delta^{18}O_{H_2O}$ signatures during the MAM rains were significantly depleted compared to both the dry season (PTT, $p =< 0.001$, $n = 15$) and the OND rains (PTT, $p = 0.001$, $n = 17$). Over a one year sampling period at S20, a positive correlation was observed between $\delta^{18}O_{H_2O}$ and $\delta^{15}N_{PN}$ signatures (Pearson correlation, correlation coefficient = 0.436, $p = 0.0258$, $n = 26$) (Fig. 6).

POC : PN ratios varied between 5.3–21.2 (mean: 10.0 ± 3.6), 7.3–20.2 (10.4 ± 2.6) and 7.6–18.4 (11.9 ± 2.5) during the dry season, OND and MAM rains, respectively. MAM rains had significantly higher POC : PN ratio than both the dry season (PTT, $p = 0.01$, $n = 19$) and the OND rains (PTT, $p = 0.003$, $n = 23$). The POC : PN ratio generally increased downstream during the dry season and OND rains, with greater altitudinal variability displayed in the MAM rains, while tributaries usually displayed higher values than main channel sites of similar altitude.

Considerable variation was observed in pelagic PP and community R rates between the dry season and the two rain seasons, particularly in the lower reaches of the main channel (Fig. 7). However, 13 of 25 OND and 10 of 23 MAM PP measurements were below detection limits, recording < 1 ‰ change between initial and final $\delta^{13}C_{POC}$. Dry season R rates were significantly higher than during OND rains (PTT, $p = 0.001$, $n = 20$) and MAM rains (PTT, $p = 0.014$, $n = 18$).

4 Discussion

The disposal of untreated waste water from the city of Nairobi has a profound impact on the A–G–S river network, leading to low O_2 levels, high NH_4^+ and high CH_4 at S1 in Athi. The highest CH_4 saturation levels (336 440 %, April 2012 at S1) is well above published values in the main stream of other African rivers such as 9600 % in the Comoé river (Koné et al., 2010), 10 600 % in the Bia river (Koné et al., 2010), 15 700 % in the Tanoé river (Koné et al., 2010), and 8900 % in the Oubangui river (Bouillon et al., 2012), and also relatively unpolluted temperate rivers such as the Ohio (10 000 %, Beaulieu et al., 2012). Yet, these CH_4 saturation values in the river main streams remain below those

BGD
10, 8637–8683, 2013

reported in the Amazon flood plains (up to 500 000 % (Richey et al., 1988; Bartlett et al., 1990). The high CH_4 saturation levels downstream of Nairobi are a signature of organic carbon pollution from waste water disposal, as also observed in the vicinity of Abidjan leading to more modest CH_4 saturation levels of 20 000 % (Koné et al., 2010) and in the Adyar River strongly polluted by the city of Chennai, with a massive CH_4 saturation level of 19 300 000 % (Rajkumar et al., 2008).

Water residence time exerts a major control on the quantity of reactive N removed by streams and rivers, whereby a longer water residence time creates greater opportunity for physical (e.g. deposition) and biological processes (e.g. nitrification, denitrification and primary production) (McGuire and McDonnell, 2007). This is clearly evident in the seasonal differences in longitudinal DIN profiles (Fig. 3a and b) of the A–G–S river network. During all seasons, headwater urban and industrial effluents and agricultural runoff supply substantial quantities of DIN to Fourteen Falls (S1), with the higher concentration during the dry season likely due to decreased dilution of waste water inputs. As a result of decreased water residence time during periods of higher discharge, DIN is largely flushed (principally as NO_3^-) directly through the A–G–S catchment. Conversely, longer water residence time during the dry season provides the basis for substantial removal of DIN above 450 m, resulting in significantly lower DIN export to the ocean under low discharge conditions. Despite the lack of high-frequency DIN data at the outlet of the A–G–S catchment, or the availability of discharge data over the sampling period, it is apparent that these seasonal DIN export observations agree with the suggestion of Dunne (1979) that as much as 80 % of the annual sediment yield in Kenyan catchments may be exported by the highest 10 % of daily flows.

In-situ increases of TA can occur through ammonification (Abril and Frankignoulle, 2001), intense NO_3^- removal by denitrification (Thomas et al., 2009) and through the intense assimilation of DIN by primary producers (Brewer and Goldman, 1976), whereas TA can be lowered due to intense NH_4^+ removal by nitrification (Frankignoulle et al., 1996). The observed increase of TA between S1 and S2 (2.16 mmol kg^{-1} to 2.76 mmol kg^{-1}, respectively) during the dry season appears contrary to DIN

BGD
10, 8637–8683, 2013

observations of intense nitrification over this reach, where loss of NH_4^+ (1012 µmol L^{-1}) is closely mirrored by production of the NO_3^- (856 µmol L^{-1}), which should lead to a decrease in TA. The low POC : PN at S1 (5.3) is indicative of the expected organic waste inputs from upstream, while the rapid loss of bulk POC from S1 (17.3 mg L^{-1}) to S2 (3.9 mg L^{-1}) suggests mineralization of this material and release of NH_4^+ by ammonification. Production of 1 mmol of NH_4^+ by ammonification creates 1 mmol of TA (Abril and Frankignoulle, 2001). Accordingly, the potential ammonification of the PN removed between S1 and S2 (2.5 mg L^{-1}) would increase TA by 0.18 mmol kg^{-1}, accounting for only 30 % of the observed increase in TA. Pelagic PP decreases rapidly from 472 µmol C L^{-1} d^{-1} at S1 to 29 µmol C L^{-1} d^{-1} at S2, so we may assume it contributes insignificantly to the increase of TA at S2. However, water hyacinth (*Eichhornia crassipes*) was observed to completely cover the dry season water surface over hundreds of meters between S1 and S2, and should be expected to significantly remove DIN and consequently increase TA, whereas these macrophytes were absent during the rain seasons when TA was observed to decrease over the corresponding reach. Notably, the rapid accumulation of N_2O over this reach (from 260 % saturation at S1 to 2855 % saturation at S2) suggests intense bacterial denitrification of available NO_3^- must be, in combination with ammonification and removal by macrophytes, the controlling factor increasing TA.

In addition to the NH_4^+ produced by the ammonification of PN between S1 and S2 during the dry season (potentially 179 µmol NH_4^+ – N L^{-1}), a further 1012 µmol L^{-1} of the initial (entering at S1) NH_4^+ pool is transformed or lost from the system along this reach. To estimate NH_4^+ transformation and loss we employed a simple formula:

$$NH_4^+ \text{ loss} = \left(\Delta NH_4^+ + A_{NH_4^+}\right) \Big/ \left(\frac{(D/V)}{t}\right) \tag{3}$$

where ΔNH_4^+ is downstream change in NH_4^+ concentration (µmol L^{-1}), $A_{NH_4^+}$ equals the NH_4^+ produced by ammonification (assuming all PN is transformed to NH_4^+), D the

BGD
10, 8637–8683, 2013

distance (m) between the sites, V the average water velocity (dry season = 0.45 m s^{-1}, OND rains = 0.82 m s^{-1}, MAM rains = 1.16 m s^{-1}; calculated from available discharge data between 1980 to 2008), and t as a time factor to convert to a daily loss rate. Between S1 and S2 we estimate a NH_4^+ loss of 1248 µmol N L^{-1} d^{-1}. Based on in-situ pelagic PP measurements at S1 and S2, and employing the Redfield C : N ratio, an estimated 4–71 µmol N L^{-1} d^{-1} is being removed by pelagic primary producers over the same reach. If we assume NH_4^+ is solely utilised by primary producers over NO_3^-, pelagic PP accounts for only 0.3–5.7 % of estimated NH_4^+ loss. The interaction of NH_4^+ or NO_3^- uptake by primary producers and any associated "preferences" or "inhibitions" is complex, and often dependant on species composition and environmental conditions (Dortch, 1990), though by assuming any NO_3^- uptake occurs during pelagic PP this only further decreases the percent NH_4^+ loss explained by this process. The heavy enrichment of $\delta^{15}N_{PN}$ along this reach, as discussed later, also points towards intense nitrification as the main factor controlling NH_4^+ removal. Hence, we hypothesize that NH_4^+ entering the study area at S1 (including NH_4^+ produced by ammonification between S1 and S2) is largely nitrified by S2, while unquantified, though significant, NO_3^- removal by denitrification is producing elevated N_2O saturation levels and simultaneously increasing TA in combination with DIN removal by pelagic PP and floating macrophytes. It is worth noting that the dense coverage of the water surface by macrophytes during the dry season may inhibit the outgassing of N_2O to the atmosphere, thereby sustaining elevated N_2O saturation levels relative to periods of their absence, such as under conditions of higher discharge during the rain seasons.

Mean NO_3^- concentration observed in the A–G–S River over the three campaigns (172.3 ± 198.2 µmol L^{-1}) is considerably higher relative to other African river catchments (Fig. 8; data not included in figure: Isinuka Springs, South Africa: 8.1 µmol L^{-1}, Faniran et al., 2001; Berg River, South Africa: 1.1–13.4 µmol L^{-1}, de Villiers, 2007; Comoé River, Ivory Coast, mean: 11.3 ± 4.4 µmol L^{-1}, Bia River, Ivory Coast, mean: 11.2 ± 4.1 µmol L^{-1}, Tanoé River, Ivory Coast, mean: 13.9 ± 5.4 µmol L^{-1}, Koné et al.,

BGD
10, 8637–8683, 2013

2009; Densu River, Ghana, mean: $33.4 \pm 0.2\,\mu mol\,L^{-1}$, Fianko et al., 2010; Upper Ewaso Ng'iro River Basin, Kenya: $0.5–27.4\,\mu mol\,L^{-1}$, Mutisya and Tole, 2010). The substantial NO_3^- loss observed between S2 and S13 during the dry season may be explained by pelagic PP assimilation of NO_3^- and/or removal by denitrifying bacteria. Assuming pelagic PP occurs only during daylight hours (12 h) and throughout the entire dry season water column (mean depth < 0.5 m), a basic comparison between daily in-situ primary production rates and total NO_3^- loss can assist in identifying the more dominant process. A simple formula was employed for calculating daily NO_3^- loss ($\mu mol\,NO_3^-\,L^{-1}\,d^{-1}$) between consecutive sites:

$$NO_3^-\ \text{loss} = \left(\Delta NO_3^- \Big/ \left(\frac{(D/V)}{t}\right)\right) \tag{4}$$

where NO_3^- is the concentration difference ($\mu mol\,L^{-1}$) between the upstream and downstream sites, D the distance (m) between the sites, V being average water velocity ($0.45\,m\,s^{-1}$; calculated from available discharge data for 1980–2008 (late dry season months = August, September, October; $n = 85$) from gauging stations (between S1 and S13)), and t a time factor for converting to daily uptake rates. Again employing the Redfield C : N to convert PP carbon uptake to PP nitrogen uptake, it is clear that pelagic primary production cannot account for the considerable NO_3^- loss in these upper reaches (Table 1), though becomes increasingly explanative downstream of S6. We have assumed here that pelagic PP is solely assimilating NO_3^-, opposite to nitrification loss calculations above, as any NH_4^+ assimilation will only decrease our estimate for removal of NO_3^- by primary producers. No *Eichhornia crassipes* blooms were observed over these reaches, and hence we assume the removal by instream macrophytes is minimal. Therefore, we hypothesize that the majority of NO_3^- formed from nitrification between S1 and S2 is removed from the system over the following 240 km, initially by intense denitrification between S2 to S6 followed by considerable pelagic PP assimilation between S6 and S13.

BGD
10, 8637–8683, 2013

N_2O is formed as a by-product of nitrification, the yield of N_2O production being a function of O_2 content (Goreau et al., 1980). Under strictly anoxic conditions, N_2O is removed by denitrification, but in the presence of O_2, denitrification leads to the accumulation of N_2O. While removal of N_2O by denitrification is a common feature in anoxic layers of lakes (Mengis et al., 1997), it has been less documented in rivers, where denitrification is assumed to be principal source of N_2O (Beaulieu et al., 2011). For instance, Amazon floodplains were found to be sinks of atmospheric N_2O (Richey et al., 1988). In the highly polluted Adyar River, N_2O is also removed below atmospheric equilibrium by denitrification on some occasions (Rajkumar et al., 2008). Overall, the N_2O content in rivers is positively related to DIN (Zhang et al., 2010; Barnes and Upstill-Goddard, 2011; Baulch et al., 2011). The high N_2O content in the DIN enriched Athi is consistent with these patterns. The only other published N_2O data-set in African rivers also agrees with these patterns, as N_2O levels are close to atmospheric equilibrium in the Oubangui river (Bouillon et al., 2012) characterized by low DIN values (mean NH_4^+ $10.4 \pm 4.9\,\mu mol\,L^{-1}$, mean NO_3^- $4.2 \pm 4.4\,\mu mol\,L^{-1}$, own unpublished data). It is not possible to discern the relative importance of N_2O production from nitrification and denitrification in the present data set, although we speculate that in rivers strongly enriched in NH_4^+ due to lack of sewage treatment, nitrification may be a strong source of N_2O, unlike temperate rivers were DIN inputs are mainly due to NO_3^- leaching from cropland, and where denitrification is assumed to be the main source of N_2O (Beaulieu et al., 2011).

DIN derived from N_2 fixation typically has $\delta^{15}N$ values 0‰ to +2‰, whereas the degradation and cycling of organic matter in waste water may yield $\delta^{15}N_{DIN}$ values towards +22‰. These enriched values are a result of the volatilization of ^{15}N-depleted NH_4^+, whilst the remaining NH_4^+ may be subsequently oxidized to ^{15}N-enriched NO_3^- (Kendall et al., 2007). Organic matter decomposition and intense nitrification between S1 and S3 results in the rapid enrichment of the residual N source (from +3.1‰ to +19.3‰, respectively). Our results are in line with Kreitler (1979), who suggest the conversion of animal waste (with a $\delta^{15}N$ value of about +5‰) to NO_3^- results in $\delta^{15}N$

BGD
10, 8637–8683, 2013

values generally between +10‰ to +20‰, validating the influence of terrestrially-derived organic waste on N-inputs within the upper A–G–S catchment. We observed minimal change in $\delta^{15}N_{PN}$ values between S3 and S6, which may be explained by the lack of assimilation of DIN by phytoplankton in the water column, evidenced by the low primary production rates observed over this reach. Additionally, the intense denitrification between S3 and S6 may not result in further significant alteration of water column ^{15}N values. Indeed, previous work has suggested minimal fractionation (−1.5‰ to −3.6‰) occurs during benthic denitrification as the water-sediment interface diffusion of NO_3^- is the rate-limiting step, which in itself causes little fractionation (Sebilo et al., 2003; Lehmann et al., 2004).

The increase of $\delta^{15}N_{PN}$ between S6 and S13 during the dry season may be attributed to the pelagic assimilation of the residual ^{15}N-enriched DIN by primary producers, as evidenced by Cole et al. (2004) who found a strong correlation between the relative contribution of waste water to stream flow and $\delta^{15}N$ values of aquatic primary producers. The higher %POC : TSM and low POC : PN observed over these sites are consistent with the presence of high phytoplankton biomass and, although logistical constraints did not allow for chlorophyll *a* measurement, the water along these reaches was stained a characteristic green hue. These findings are consistent with di Persia and Neiff (1986), who suggest that highest phytoplankton biomass density in tropical rivers occurs during the dry season, when water residence time is greatest and turbidity is minimal, with similar patterns between dry and wet season biomass densities also observed in tropical rivers of Ivory Coast (Lévêque, 1995; Koné et al., 2009), Asia (Dudgeon, 1995) and Australia (Townsend et al., 2011). By S13 a combination of intense denitrification and enhanced pelagic primary production lower DIN to levels equivalent to observations in other African river catchments (see Fig. 8), whilst simultaneously these processes enriched $\delta^{15}N_{PN}$ to values not previously recorded in Africa river catchments (Fig. 9).

Between S13 and S20 pelagic primary production rates gradually decline with a concomitant decrease in %POC : TSM, $\delta^{15}N_{PN}$ and increasing POC : PN. Following the

BGD
10, 8637–8683, 2013

confluence of the Tsavo with the A–G–S above S14, there are no further tributaries contributing flow during the dry season along this reach, and hence the above observations cannot be a factor of gradual dilution by terrestrially sourced TSM, but are likely to result from instream transformation of the C and N pools. Two sources of TSM are considered for the A–G–S system, terrestrially produced TSM with characteristically low %POC : TSM and high POC : PN, and autochthonous TSM in the form of algal biomass, represented by high %POC : TSM and low POC : PN. Our most likely hypothesis to explain the downstream trends in %POC, POC/PN, and $\delta^{15}N_{PN}$ signatures is the preferential loss of the more labile, ^{15}N-enriched algal biomass pool. In order to test this hypothesis, we attempted to fit a two source mixing model to field observations between S13 and S20, where a pure autochthonous source was defined by %POC : TSM of 40, POC : PN represented by the Redfield ratio, and a $\delta^{15}N_{PN}$ of +32‰, a value marginally enriched relative to field observations (+31.5‰ at S13). Under dry season conditions, we would expect minimal contribution of soil erosion to the terrestrial source, whereas much of the dry season OC may be sourced from upstream organically enriched waste water sources. The best fit to the data was found by employing a terrestrial POC : PN of 18, i.e., considerably lower than reported terrestrial C : N ratios (e.g. mean = 36, Elser et al., 2000) but in line with expected degradation within the aquatic system, and a terrestrial $\delta^{15}N_{PN}$ of +5‰. Assuming an initial proportion of autochthonous : terrestrial sourced TSM of 85 : 15, and simulating the effect of gradual decomposition of the labile (autochthonous) component while the (less labile) terrestrial component remained intact and in transit, the mixing model output provided a good relationship with observed POC : PN and $\delta^{15}N_{PN}$ (Fig. 10a). Likewise, a suitable match is established between field observations and mixing model output for %POC : TSM and $\delta^{15}N_{PN}$ (Fig. 10b) when employing the above constraints and a terrestrial %POC : TSM end member of 8. Although the terrestrial %POC : TSM end member is relatively high, it provides the best fit with field observations in this situation and is partially justified by the prevailing high organic waste water loading. We speculate that the preferential decomposition of more labile autochthonous organic matter, relative to more recalcitrant

BGD
10, 8637–8683, 2013

terrestrial materials, is largely driving the %POC : TSM lower and POC : PN ratio higher along this lower reach, which in turn leads to depletion of ^{15}N within the PN pool. Bouillon et al. (2009) and Tamooh et al. (2012) reported similar rapid loss of phytoplankton biomass in the bordering Tana River, as well as Zurbrügg et al. (2013) in the Kafue River, Zambia, albeit downstream of reservoirs under both these studies. As the quantity of (^{15}N-enriched) phytoplankton biomass decreases in the A–G–S the $\delta^{15}N_{PN}$ gradually becomes more depleted, though still discharging to the Indian Ocean a $\delta^{15}N$ signature (+17.0‰) evidently imprinted by human-induced N input to the A–G–S headwaters.

$\delta^{15}N_{PN}$ during the rain seasons are lower and less variable than during the dry season, likely due to the decreased residence time of water from source to outlet and consistent with the lower degree of DIN processing. Although corresponding discharge measurements were unavailable, data from ongoing bi-weekly sampling at the most downstream station (S20) show a strong relationship between $\delta^{15}N_{PN}$ and seasonal variations in the hydrograph. Seasonal variation in rainfall is suggested as the cause of $\delta^{18}O_{H_2O}$ increases observed in stream water under dry season conditions, during which the water is predominantly composed of old groundwater of essentially constant isotopic signature, whereas during rain seasons this signature becomes mixed with the more depleted signature of catchment precipitation (Mook and De Vries, 2000). Employing our bi-weekly $\delta^{18}O_{H_2O}$ data as a proxy indicator for river discharge, we found a positive correlation with $\delta^{15}N_{PN}$ at the outlet of the A–G–S River (Fig. 6). A more acceptable linear fit was observed when shifting the $\delta^{18}O_{H_2O}$ observations forward one month relative $\delta^{15}N_{PN}$ observations, which is likely a time delay associated with N transformation as a result of the changing hydrograph (e.g. time required for sufficient assimilation of enriched ^{15}N to be observed within the PN pool). Hence, the enriched $\delta^{15}N_{PN}$ export during the dry season, and likewise the more depleted $\delta^{15}N_{PN}$ export during rain seasons, clearly reflect the extent of internal N cycling in the upper catchment under varying flow regimes.

BGD
10, 8637–8683, 2013

As outlined earlier, the A–G–S catchment has undergone considerable land-use change in the past century, largely as a result of increased population pressure and associated resource demands placed on the region. Ba/Ca ratios in Malindi reef corals, collected from the coastal surrounds of the A–G–S catchment, have previously been employed to reconstruct a 300 yr timeline of increasing sediment flux to the ocean (Fleitmann et al., 2007), linked to exacerbated soil erosion associated with intensified land-use, cultivation of steep slopes, deforestation for wood fuel production, urban sprawl and expanding rural (largely unsealed) road networks throughout the catchment. Ohowa (1996), similarly to our results, observed peaks in NO_3^- export at the A–G–S outlet during the MAM and OND rains, though their peak NO_3^- measurement (1.4 µmol L^{-1}; 1991 OND rains) was more than two magnitudes lower than our peak observation (530.7 µmol L^{-1}; 2011 OND rains) two decades later. The reason for discrepancy between results is ambiguous. Assuming no measurement error on the part of Ohowa (1996), we may interpret the difference as a very rapid increase of NO_3^- export from the A–G–S catchment over the last 20 yr. The insufficient development of sewage and sanitation services to match the burgeoning Nairobi population, having more than doubled over the two decades between work of Ohowa (1996) and the present study, provides some insight to the possible driver of the substantial increase observed in NO_3^- export.

The Global News2 dataset (Mayorga et al., 2010) predicts TSM load and PN load of 42.73 million t yr^{-1} 38 764 956 Mg yr^{-1} and 18.13 million t yr^{-1} 16 445 Mg yr^{-1} for the A–G–S outlet, respectively, equating to a %PN : TSM of 0.04. This is considerably less than the average value of 0.31 %PN : TSM for our measurements calculated over a one year sampling interval (28 measurements). Mayorga et al. (2010) first estimate TSM load and then use empirical relationships observed between TSM and %PN : TSM to estimate PN load. Local conditions of N-loading in the A–G–S system, as outlined above, are not taken in account by the Global News2 estimates, which likely results in the discrepancy between the empirical calculations and our field derived observations.

BGD
10, 8637–8683, 2013

Hence, caution should prevail when employing these broad-scale modelling relationships to heavily disturbed systems such as the A–G–S catchment.

Our δ^{15}N data display the impact of human-induced disturbance on the watershed N cycle within the A–G–S catchment, embedding a "disturbance" signature within the exported particulate N. Potential exists for employing the δ^{15}N values of sediments, bivalves and corals from within the catchment and marine environment surrounding the river mouth as proxy indicators for the historical evolution of N sources to the A–G–S catchment consequent to prevailing land-use changes. Elliot and Bush (2006) related an increase in $\delta^{15}N_{org}$ values from +2‰ to +7‰ in a freshwater wetland sediment core spanning 350 yr to changes in land-use from forested conditions to increasing nutrient inputs from human wastes. Likewise, coring of coral heads and extraction of δ^{15}N values could provide timelines extending from centuries to millennia (Marion et al., 2005). Alternatively, the δ^{15}N in the growth tips of Gorgonians (coral fans) have proved to closely reflect the food (N) source of the organism (Risk et al., 2009), with many species forming annual growth rings (Grigg, 1974) which can remain chemically stable for a period of time following death (Goldberg and Hamilton, 1974; Goldberg, 1976; Sherwood et al., 2005). Similarly, the growth pattern of bivalves provides a timeline of the evolution of the organisms' external environment, with potential preservation of the organic matrix for thousands of years under favorable conditions (Weiner et al., 1979; Risk et al., 1997). With species-specific lifespans exceeding 50 yr, an organism may store proxies of pre-disturbance terrestrial conditions in recently disturbed environments. With the proximity of Malindi–Watamu reef to the A–G–S outlet, there should exist a plethora of submerged marine biological proxies which could assist in creating a δ^{15}N timeline of land-use change within the A–G–S catchment. The sediment-laden nature of the A–G–S river and the associated infilling of the Sabaki estuary, first recognized by Oosterom (1988), likewise may store a comprehensive δ^{15}N timeline of catchment evolution. The relatively low-cost nature of these techniques is an added benefit for their use in economically-challenged, developing countries where little baseline data exists (Risk et al., 2009).

BGD
10, 8637–8683, 2013

5 Conclusions

Nitrogen-loading of the A–G–S headwaters surrounding Nairobi leads to strong seasonal N-cycling dynamics dependant on the prevailing discharge regime. High discharge during rain seasons results in the rapid flushing of large quantities of DIN from the headwaters to the outlet, whereas increased water residence time during the dry season permits substantial transformation and removal of DIN in the upper- to mid-catchment (Fig. 11). The decomposition of headwater OM waste inputs during the dry season provides a large volume of DIN which undergoes intense nitrification in the upper reaches, producing elevated NO_3^- concentrations, significant N_2O and enriched $\delta^{15}N_{PN}$, while concomitant denitrification leads to further N_2O outgassing to the atmosphere. Over the following 240 km, a combination of benthic denitrification and pelagic primary production efficiently lower NO_3^- levels to that observed in most other African catchments, whilst associated fractionation further enriches $\delta^{15}N_{PN}$. Availability of labile OM and coupled nitrification-denitrification in the shallow water column maintains elevated instream metabolism in the lower reaches, with the river discharging significantly diminished DIN concentrations, relative to upstream inputs, during low flow conditions. The strong correlation found between seasonal $\delta^{15}N_{PN}$ and discharge regime presents the possibility of employing mutually beneficial proxy indicators, such as a combination of $\delta^{15}N_{PN}$ of sediments, corals and bivalves, to build the foundation of how historical land-use changes have influenced N cycling within the catchment.

Supplementary material related to this article is available online at: http://www.biogeosciences-discuss.net/10/8637/2013/ bgd-10-8637-2013-supplement.pdf.

BGD
10, 8637–8683, 2013

Acknowledgements. Funding for this work was provided by the European Research Council (ERC-StG 240002, AFRIVAL, http://ees.kuleuven.be/project/afrival/), and by the Research Foundation Flanders (FWO-Vlaanderen, project G.0651.09). We thank Zita Kelemen (KU Leuven), Peter Salaets (KU Leuven), and Marc-Vincent Commarieu (ULg) for technical and laboratory assistance, Matheka Kioko (Kenya Wildlife Service) for field assistance during the seasonal sampling campaigns, and John Ngilu (Water Resource Management Authority, Machakos, Kenya) for providing the discharge data for various A–G–S gauging stations. Data in the Ogooué (Gabon) were collected by Jean-Daniel Mbega (Institut de Recherches Agronomiques et Forestières, Libreville, Gabon) and data in the Niger were collected by Alhou Bassirou (Univerté de Niamey, Niamey, Niger). A. V. B. is a research associate at the FRS-FNRS (Belgium).

References

Abril, G. and Frankignoulle, M.: Nitrogen–alkalinity interactions in the highly polluted Scheldt basin (Belgium), Water Res., 35, 844–850, 2001.

Aravena, R., Evans, M. L., and Cherry, J. A.: Stable isotopes of oxygen and nitrogen in source identification of nitrate from septic systems, Ground Water, 31, 180–186, 1993.

Ayres, R. U., Schlesinger, W. H., and Socolow, R. H.: Human impacts on the nitrogen cycle, in: Industrial Ecology and Global Change, edited by: Socolow, R., Andrews, C., Berkhout, F., and Thomas, V., Cambridge University Press, Cambridge, UK, 121–155, 1994.

Bartlett, K. B., Crill, P. M., Bonassi, J. A., Richey, J. E., and Harris, R. C.: Methane flux from the Amazon River floodplain: emissions during rising water, J. Geophys. Res., 95, 16773–16778, doi:10.1029/JD095iD10p16773, 1990.

Barnes, J. and Upstill-Goddard, R. C.: N_2O seasonal distributions and air-sea exchange in UK estuaries: implications for the tropospheric N_2O source from European coastal waters, J. Geophys. Res., 116, G01006, doi:10.1029/2009JG001156, 2011.

Baulch, H. M., Schiff, S. L., Maranger, R., and Dillon, P. J.: Nitrogen enrichment and the emission of nitrous oxide from streams, Global Biogeochem. Cy., 25, GB4013, doi:10.1029/2011GB004047, 2011.

Beaulieu, J. J., Tank, J. L., Hamilton, S. K., Wollheim, W. M., Hall Jr., R. O., Mulholland, P. J., Peterson, B. J., Ashkenas, L. R., Cooper, L. W., Dahm, C. N., Dodds, W. K., Grimm, N. B., Johnson, S. L., McDowell, W. H., Poole, G. C., Valett, H. M., Arango, C. P., Bernot, M. J.,

Burgin, A. J., Crenshaw, C. L., Helton, A. M., Johnson, L. T., O'Brien, J. M., Potter, J. D., Sheibley, R. W., Sobota, D. J., and Thomas, S. M.: Nitrous oxide emission from denitrification in stream and river networks, P. Natl. Acad. Sci. USA, 108, 214–219, 2011.

Beaulieu, J. J., Shuster, W. D., and Rebholz, J. A.: Controls on gas transfer velocities in a large river, J. Geophys. Res., 117, G02007, doi:10.1029/2011JG001794, 2012.

Bouillon, S., Abril, G., Borges, A. V., Dehairs, F., Govers, G., Hughes, H. J., Merckx, R., Meysman, F. J. R., Nyunja, J., Osburn, C., and Middelburg, J. J.: Distribution, origin and cycling of carbon in the Tana River (Kenya): a dry season basin-scale survey from headwaters to the delta, Biogeosciences, 6, 2475–2493, doi:10.5194/bg-6-2475-2009, 2009.

Bouillon, S., Yambélé, A., Spencer, R. G. M., Gillikin, D. P., Hernes, P. J., Six, J., Merckx, R., and Borges, A. V.: Organic matter sources, fluxes and greenhouse gas exchange in the Oubangui River (Congo River basin), Biogeosciences, 9, 2045–2062, doi:10.5194/bg-9-2045-2012, 2012.

Bouwman, A. F., Van Drecht, G., Knoop, J. M., Beusen, A. H. W., and Meinardi, C. R.: Exploring changes in river nitrogen export to the world's oceans, Global Biogeochem. Cy., 19, GB1002, doi:10.1029/2004GB002314, 2005.

Brewer, P. G. and Goldman, J. C.: Alkalinity changes generated by phytoplankton growth, Limnol. Oceanogr., 21, 108–117, 1976.

Canfield, D. E., Glazer, A. N., and Falkowski, P. G.: The evolution and future of Earth's nitrogen cycle, Science, 330, 192–196, doi:10.1126/science.1186120, 2010.

Cao, H., Auguet, J.-C., and Gu, J.-D.: Global ecological pattern of ammonia-oxidizing archaea, PLoS ONE 8, e52853, doi:10.1371/journal.pone.0052853, 2013.

Caraco, N. F. and Cole, J. J.: Human impact on nitrate export: an analysis using major world rivers, Ambio, 28, 167–170, 1999.

Carpenter, S. R., Caraco, N. F., Correll, D. L., Howarth, R. W., Sharpley, A. N., and Smith, V. H.: Nonpoint pollution of surface waters with phosphorus and nitrogen, Ecol. Appl., 8, 559–568, 1998.

Cole, M. L., Valiela, I., Kroeger, K. D., Tomasky, G. L., Cebrian, J., Wigand, C., McKinney, R. A., Grady, S. P., and Carvalho da Silva, M. H.: Assessment of a δ^{15}N isotopic method to indicate anthropogenic eutrophication in aquatic ecosystems, J. Environ. Qual., 33, 124–132, 2004.

Dafe, F.: No business like slum business? The political economy of the continued existence of slums: a case study of Nairobi, DESTIN: Development Studies Institute, Working Paper Series, No. 09-98, 2009.

BGD
10, 8637–8683, 2013

De Brabandere, L., Dehairs, F., Van Damme, S., Brion, N., Meire, P., and Daro, N.: δ^{15}N and δ^{13}C dynamics of suspended organic matter in freshwater and brackish waters of the Scheldt estuary, J. Sea Res., 48, 1–15, 2002.

de Villiers, S.: The deteriorating nutrient status of the Berg River, South Africa, Water SA, 33, 659–664, 2007.

di Persia, D. H. and Neiff, J. J.: The Uruguay river system, in: The Ecology of River Systems, edited by: Davies, B. R., Walker, K. F., and Junk, W., Dordrecht, the Netherlands, 599–620, 1986.

Downing, J. A., McClain, M., Twilley, R., Melack, J. M., Elser, J., Rabalais, N. N., Lewis Jr., W. M., Turner, R. E., Corredor, J., Soto, D., Yanez-Arancibia, A., Kopaska, J. A., and Howarth, R. W.: The impact of accelerating land-use change on the N-cycle of tropical aquatic ecosystems: current conditions and projected changes, Biogeochemistry, 46, 109–148, 1999.

Dudgeon, D.: The ecology of rivers and streams in tropical Asia, in: River and Stream Ecosystems,edited by: Cushing, C. E., Cummins K. W., and Minshall, G. W., Elsevier Science B.V., Amsterdam, 615–657, 1995.

Dunne, T.: Sediment yield and land use in tropical catchments, J. Hydrol., 42, 281–300, 1979.

Elliot, E. M. and Brush, G. S.: Sedimented organic nitrogen isotopes in freshwater wetlands record long-term changes in watershed nitrogen source and land use, Environ. Sci. Technol, 40, 2910–2916, 2006.

Faniran, J. A., Ngceba, F. S., Bhat, R. B., and Oche, C. Y.: An assessment of the water quality of the Isinuka springs in the Transkei region of the Eastern Cape, Republic of South Africa, Water SA, 27, 241–250, 2001.

Fianko, J. R., Lowor, S. T., Donkor, A., and Yeboah, P. O.: Nutrient chemistry of the Densu River in Ghana, Environmentalist, 30, 145–152, 2010.

Fleitmann, D., Dunbar, R. B., McCulloch, M., Mudelsee, M., Vuille, M., McClanahan, T. R., Cole, J. E., and Eggins, S.: East African soil erosion recorded in a 300 year old coral colony from Kenya, Geophys. Res. Lett., 34, L04401, doi:10.1029/2006GL028525, 2007.

Frankignoulle, M., Bourge, I., and Wollast, R.: Atmospheric CO_2 fluxes in a highly polluted estuary (the Scheldt), Limnol. Oceanogr., 41, 365–369, 1996.

French, E., Kozlowski, J. A., Mukherjee, M., Bullerjahn, G., and Bollmanna, A.: Ecophysiological characterization of ammonia-oxidizing archaea and bacteria from freshwater, Appl. Environ. Microb., 78, 5773–5780, 2012.

BGD
10, 8637–8683, 2013

Galloway, J. N. and Cowling, E. B.: Reactive nitrogen and the world: 200 years of change, AMBIO, 31, 64–71, 2002.
Galloway, J. N., Schlesinger, W. H., Hiram Levy, I. I., Michaels, A., and Schnoor, J. L.: Nitrogen fixation: anthropogenic enhancement-environmental response, Global Biogeochem. Cy., 9, 235–252, 1995.
Galloway, J. N., Aber, J. D., Erisman, J. W., Seitzinger, S. P., Howarth, R. W., Cowling, E. B., and Cosby, B. J.: The nitrogen cascade, Bioscience, 53, 341–356, 2003.
Gillikin, D. P. and Bouillon, S.: Determination of δ^{18}O of water and δ^{13}C of dissolved inorganic carbon using a simple modification of an elemental analyser-isotope ratio mass spectrometer: an evaluation, Rapid Commun. Mass Sp., 21, 1475–1478, 2007.
Goldberg, W. M.: Comparative study of the chemistry and structure of gorgonian and antipatharian coral skeletons, Mar. Biol., 35, 253–267, 1976.
Goldberg, W. M. and Hamilton, R. D.: The sexual cycle in Plexaura homomalla, in: Prostoglandins from Plexaura Homomalla: Ecology, Utilization and Conservation of a Major Medical Marine Resource, a Symposium, edited by: Bayer, M. and Weinheimer, A. J., University of Miami Press, Miami, FL, 58–61, 1974.
Goreau, T. J., Kaplan, W. A., Wofsy, S. C., McElroy, M. B., Valois, F. W., and Watson, S. W.: Production of NO_2^- and N_2O by nitrifying bacteria at reduced concentrations of oxygen, Appl. Environ. Microb., 40, 526–532, 1980.
Green, P. A., Vörösmarty, C. J., Meybeck, M., Galloway, J. N., Peterson, B. J., and Boyer, E. W.: Pre-industrial and contemporary fluxes of nitrogen through rivers: a global assessment based on typology, Biogeochemistry, 68, 71–105, 2004.
Grigg, R. W.: Growth rings: annual periodicity in two gorgonian corals, Ecology, 55, 876–881, 1974.
Harrison, J. A., Maranger, R. J., Alexander, R. B., Giblin, A. E., Jacinthe, P. A., Mayorga, E., Seitzinger, S. P., Sobota, D. J., and Wollheim, W. M.: The regional and global significance of nitrogen removal in lakes and reservoirs, Biogeochemistry, 93, 143–157, 2009.
Holland, E. A., Dentener, F. J., Braswell, B. H., and Sulzman, J. M.: Contemporary and pre-industrial global reactive nitrogen budgets, Biogeochemistry, 46, 7–43, 1999.
Howarth, R. W.: Coastal nitrogen pollution: a review of sources and trends globally and regionally, Harmful Algae, 8, 14–20, 2008.
Howarth, R. W., Billen, G., Swaney, D., Townsend, A., Jaworski, N., Lajtha, K., Downing, J. A., Elmgren, R., Caraco, N., Jordan, T., Berendse, F., Freney, J., Kudeyarov, V., Murdoch, P.,

BGD
10, 8637–8683, 2013

and Zhao-Liang, Z.: Regional nitrogen budgets and riverine N and P fluxes for the drainages to the North Atlantic Ocean: natural and human influences, Biogeochemistry, 35, 75–139, 1996.

K.N.B.S.: Kenya: 2009 population and housing census highlights, Kenyan National Bureau of Statistics, 2009.

Kendall, C., Elliott, E. M., and Wankel, S. D.: Tracing anthropogenic inputs of nitrogen to ecosystems, in: Stable Isotopes in Ecology and Environmental Science, 2nd edn., edited by: Michener, R. and Lajtha, K., Blackwell Publishing, Malden, USA, 375–449, 2007.

Kitthia, S. M.: Land use changes and their effects on sediment transport and soil erosion within the Athi drainage basin, Kenya, IAHS-AISH P., 245, 145–150, 1997.

Kithiia, S. M.: Effects of sediments loads on water quality within the Nairobi River Basins, Kenya, Int. J. Environ. Protect., 2, 16–20, 2012.

Kithiia, S. M. and Wambua, B. N.: Temporal changes of sediment dynamics within the Nairobi River sub-basins between 1998–2006 time scale, Kenya, Annals of Warsaw University of Life Sciences – SGGW, Land Reclamation, 42, 2010.

Koné, Y. J. M., Abril, G., Kouadio, K. N., Delille, B., and Borges, A. V.: Seasonal variability of carbon dioxide in the rivers and lagoons of Ivory Coast (West Africa), Estuar. Coast., 32, 246–260, 2009.

Koné Y. J. M., Abril, G., Delille, B., and Borges, A. V.: Seasonal variability of methane in the rivers and lagoons of Ivory Coast (West Africa), Biogeochemistry, 100, 21–37, 2010.

Kreitler, C. W.: Nitrogen-isotope ratio studies of soils and groundwater nitrate from alluvial fan aquifers in Texas, J. Hydrol., 42, 147–170, 1979.

Lapointe, B. E., Barile, P. J., Littler, M. M., and Littler, D. S.: Macroalgal blooms on southeast Florida coral reefs: 2. Cross-shelf discrimination of nitrogen sources indicates widespread assimilation of sewage nitrogen, Harmful Algae, 4, 1106–1122, 2005.

Lehmann, M. F., Sigman, D. M., and Berelson, W. M.: Coupling the $^{15}N/^{14}N$ and $^{18}O/^{16}O$ of nitrate as a constraint on benthic nitrogen cycling, Mar. Chem., 88, 1–20, 2004.

Lévêque, C.: River and stream ecosystems of northwestern Africa, in: River and Stream Ecosystems,edited by: Cushing, C. E., Cummins, K. W., and Minshall, G. W., Elsevier Science B.V., Amsterdam, 519–536, 1995.

Marion, G. S., Dunbar, R. B., Mucciarone, D. A., Kremer, J. N., Lansing, J. S., and Arthawiguna, A.: Coral skeletal $\delta^{15}N$ reveals isotopic traces of an agricultural revolution, Mar. Pollut. Bull., 50, 931–944, 2005.

BGD
10, 8637–8683, 2013

McGuire, K. and McDonnell, J.: Stable isotope tracers in watershed hydrology, in: Stable Isotopes in Ecology and Environmental Science, 2nd edn., edited by: Michener, R. and Lajtha, K., Blackwell Publishers, Boston, Massachusetts, 334–374, 2007.
Mogaka, H., Gichere, S., Davis, R., and Hirji, R.: Climate variability and water resources degradation in Kenya: improving water resources development and management, World Bank Working Papers 69, 2006.
Mengis, M., Gachter, R., and Wehrli, B.: Sources and sinks of nitrous oxide (N_2O) in deep lakes, Biogeochemistry, 38, 281–301, doi:10.1023/A:1005814020322, 1997.
Mook, W. G. and De Vries, J. J.: Environmental Isotopes in the Hydrological Cycle: Principles and Applications, vol. 3, Surface Water, 2000.
Mutisya, D. K. and Tole, M.: The impact of irrigated agriculture on water quality of rivers Kongoni and Sirimon, Ewaso Ng'iro North Basin, Kenya, Water Air Soil Poll., 213, 145–149, 2010.
Mylène, H., Sandrine, E., Antoine, B., Cécile, L., Isabelle, D., Clarisse, M., Giséle, B., Didier, D., and Isabelle, M.: Dynamics of ammonia oxidizing archaea and bacteria in contrasted freshwater ecosystems, Res. Microbiol., 164, 360–370, doi:10.1016/j.resmic.2013.01.004, 2013.
Ohowa, B. O.: Seasonal variations of the nutrient fluxes into the Indian Ocean from the Sabaki river, Kenya, Discov. Innovat., 8, 265–274, 1996.
Olima, W.: Dynamics and implications of sustaining urban spatial segregation in Kenya – experiences from Nairobi metropolis, in: International Seminar on Segregation in the City, Lincoln Institute of Land Policy, World Health Organization (WHO), Cambridge, USA, 2001.
Ongwenyi, G. S., Kithiia, S. M., and Denga, F. O.: An Overview of the Soil Erosion and Sedimentation Problems in Kenya, IAHS Press, Wallingford, UK, 1993.
Oosterom, A. P.: The geomorphology of southeast Kenya, Ph. D. thesis, Agricultural University, Wageningen, the Netherlands, 1988.
Owens, N. J. P.: Natural variations in ^{15}N in the marine environment, Adv. Mar. Biol., 24, 390–451, 1987.
Rajkumar, A. N., Barnes, J., Ramesh, R., Purvaja, R., and Upstill-Goddard, R.: Methane and nitrous oxide fluxes in the polluted Adyar River and estuary, SE India, Mar. Pollut. Bull., 56, 2043–2051, doi:10.1016/j.marpolbul.2008.08.005, 2008.
Ravishankara, A. R., Daniel, J. S., and Portmann, R. W.: Nitrous oxide (N_2O): the dominant ozone-depleting substance emitted in the 21st century, Science, 326, 123–125, 2009.

BGD
10, 8637–8683, 2013

Richey, J. E., Devol, A. H., Wofy, S. C., Victoria, R., and Riberio, M. N. G.: Biogenic gases and the oxidation and reduction of carbon in Amazon River and floodplain waters, Limnol. Oceanogr., 33, 551–561, 1988.

Risk, M. J., Sayer, B. G., Tevesz, M. J., and Karr, C. D.: Comparison of the organic matrix of fossil and recent bivalve shells, Lethaia, 29, 197–202, 1997.

Risk, M. J., Lapointe, B. E., Sherwood, O. A., and Bedford, B. J.: The use of δ^{15}N in assessing sewage stress on coral reefs, Mar. Pollut. Bull., 58, 793–802, 2009.

Sebilo, M., Billen, G., Grably, M., and Mariotti, A.: Isotopic composition of nitrate-nitrogen as a marker of riparian and benthic denitrification at the scale of the whole Seine River system, Biogeochemistry, 63, 35–51, 2003.

Seitzinger, S. P. and Kroeze, C.: Global distribution of nitrous oxide production and N inputs in freshwater and coastal marine ecosystems, Global Biogeochem. Cy., 12, 93–113, 1998.

Seitzinger, S., Harrison, J. A., Böhlke, J. K., Bouwman, A. F., Lowrance, R., Peterson, B., Tobias, C., and Van Drecht, G.: Denitrification across landscapes and waterscapes: a synthesis, Ecol. Appl., 16, 2064–2090, 2006.

Seitzinger, S. P., Mayorga, E., Bouwman, A. F., Kroeze, C., Beusen, A. H. W., Billen, G., Van Drecht, G., Dumont, E., Fekete, B. M., Garnier, J., and Harrison, J. A.: Global river nutrient export: a scenario analysis of past and future trends, Global Biogeochem. Cy., 24, GB0A08, doi:10.1029/2009GB003587, 2010.

Sherwood, O. A., Scott, D. B., Risk, M. J., and Guilderson, T. P.: Radiocarbon evidence for annual growth rings in the deep-sea octocoral *Primnoa resedaeformis*, Mar. Ecol. Prog. Ser., 301, 129–134, 2005.

Tamooh, F., Van den Meersche, K., Meysman, F., Marwick, T. R., Borges, A. V., Merckx, R., Dehairs, F., Schmidt, S., Nyunja, J., and Bouillon, S.: Distribution and origin of suspended matter and organic carbon pools in the Tana River Basin, Kenya, Biogeosciences, 9, 2905–2920, doi:10.5194/bg-9-2905-2012, 2012.

Taylor, P. G. and Townsend, A. R.: Stoichiometric control of organic carbon–nitrate relationships from soils to the sea, Nature, 464, 1178–1181, 2010.

Thomas, H., Schiettecatte, L.-S., Suykens, K., Koné, Y. J. M., Shadwick, E. H., Prowe, A. E. F., Bozec, Y., de Baar, H. J. W., and Borges, A. V.: Enhanced ocean carbon storage from anaerobic alkalinity generation in coastal sediments, Biogeosciences, 6, 267–274, doi:10.5194/bg-6-267-2009, 2009.

BGD
10, 8637–8683, 2013

Tiffen, M., Mortimore, M., and Gichuki, F.: More people less erosion: environmental recovery in Kenya, ACTS Press, Nairobi, Kenya, 33–43, 1994.
Townsend, S. A., Webster, I. T., and Schult, J. H.: Metabolism in a groundwater-fed river system in the Australian wet/dry tropics: tight coupling of photosynthesis and respiration, J. N. Am. Benthol. Soc., 30, 603–620, 2011.
Trimmer, M., Grey, J., Heppell, C. M., Hildrew, A. G., Lansdown, K., Stahl, H., and Yvon-Durocher, G.: River bed carbon and nitrogen cycling: state of play and some new directions, Sci. Total Environ., 434, 143–158, 2012.
Van Katwijk, M., Meier, N. F., Loon, R. V., Hove, E. V., Giesen, W. B. J. T., Velde, G. V. D., and Hartog, C. D.: Sabaki river sediment load and coral stress: correlation between sediments and condition of the Malindi–Watamu reefs in Kenya (Indian Ocean), Mar. Biol., 117, 675–683, 1993.
Vitoria, L., Otero, N., Soler, A., and Canals, A.: Fertilizer characterization: isotopic data (N, S, O, C, and Sr), Environ. Sci. Technol., 38, 3254–3262, 2004.
Vitousek, P. M., Aber, J. D., Howarth, R. W., Likens, G. E., Matson, P. A., Schindler, D. W., Schlesinger, W. H., and Tilman, D. G.: Human alteration of the global nitrogen cycle: sources and consequences, Ecol. Appl., 7, 737–750, 1997.
Weiner, S., Lowenstam, H. A., Taborek, B., and Hood, L.,: Fossil mollusk shell organic matrix components preserved for 80 million years, Paleobiology, 5, 144–150, 1979.
Weiss, R. F.: Determinations of carbon dioxide and methane by dual catalyst flame ionization chromatography and nitrous oxide by electron capture chromatography, J. Chromatogr. Sci., 19, 611–616, 1981.
Weiss, R. F. and Price, B. A.: Nitrous oxide solubility in water and seawater, Mar. Chem., 8, 347–359, 1980.
Wetzel, R. G.: Limnology, 3rd edn., Lake and River Ecosystems, Academic Press, San Diego, 2001.
Widory, D., Petelet-Giraud, E., Negrel, P., and Ladouche, B.: Tracking the sources of nitrate in groundwater using coupled nitrogen and boron isotopes: a synthesis, Environ. Sci. Technol., 39, 539–548, 2005.
Wrage, N., Velthof, G. L., van Beusichem, M. L., and Oenema, O.: Role of nitrifier denitrification in the production of nitrous oxide, Soil Biol. Biochem., 33, 1723–1732, doi:10.1016/S0038-0717(01)00096-7, 2001.

BGD
10, 8637–8683, 2013

Yamamoto, S., Alcauskas, J. B., and Crozier, T. E.: Solubility of methane in distilled water and seawater, J. Chem. Eng. Data, 21, 78–80, 1976.

Yasin, J. A., Kroeze, C., and Mayorga, E.: Nutrients export by rivers to the coastal waters of Africa: past and future trends, Global Biogeochem. Cy., 24, GB0A07, doi:10.1029/2009GB003568, 2010.

Zhang, G.-L., Zhang, J., Liu, S.-M., Ren, J.-L., and Zhao, Y.-C.: Nitrous oxide in the Changjiang (Yangtze River) Estuary and its adjacent marine area: Riverine input, sediment release and atmospheric fluxes, Biogeosciences, 7, 3505–3516, doi:10.5194/bg-7-3505-2010, 2010.

Zurbrügg, R., Suter, S., Lehmann, M. F., Wehrli, B., and Senn, D. B.: Organic carbon and nitrogen export from a tropical dam-impacted floodplain system, Biogeosciences, 10, 23–38, doi:10.5194/bg-10-23-2013, 2013.

BGD
10, 8637–8683, 2013

Table 1. Inter-site comparison of average NO_3^- loss and pelagic primary production (PP) assimilated N in order to delineate the primary control of NO_3^- loss for sites S2 to S13 during the dry season. The calculation of average NO_3^- loss is outlined in the discussion section. The range for PP assimilated N is calculated using the upstream and downstream pelagic PP observations and converted from C uptake to N uptake using the Redfield C : N ratio. It must be stressed these are basic calculations with a number of assumptions (see text).

Site	NO_3^- loss ($\mu mol\,N\,L^{-1}\,d^{-1}$)	PP assimilated N ($\mu mol\,N\,L^{-1}\,d^{-1}$)	%N loss by PP
S2–S3	90	4–7	5–7
S3–S4	32	7–18	21–57
S4–S5	127	18–20	14–16
S5–S6	65	20–45	31–69
S6–S11	159	45–166	28–104
S11–S13	193	166–326	86–169

BGD
10, 8637–8683, 2013

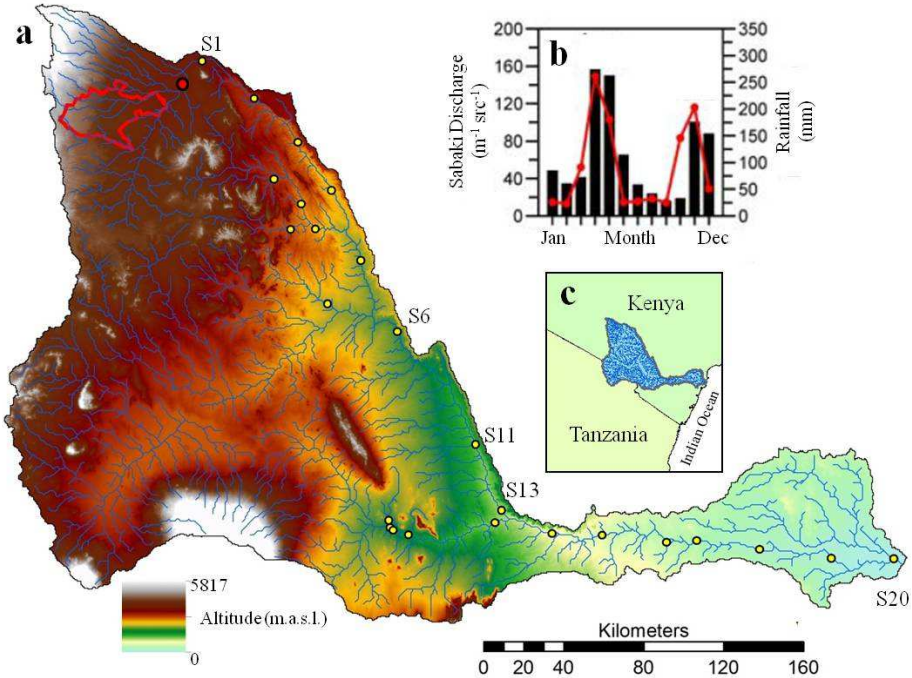

Fig. 1. (a) Digital elevation model (DEM) of Athi–Galana–Sabaki River catchment (yellow circles = sample sites; red circle = Nairobi–Athi confluence). The Nairobi administration boundary is indicated by the red outline in the DEM. **(b)** Mean monthly A–G–S discharge and precipitation (taken from Fleitmann et al., 2007), displaying the bi-modal hydrograph in connection with the long and short rain seasons. Inset map **(c)** shows the position of the A–G–S catchment within south-eastern Kenya and north-eastern Tanzania.

BGD
10, 8637–8683, 2013

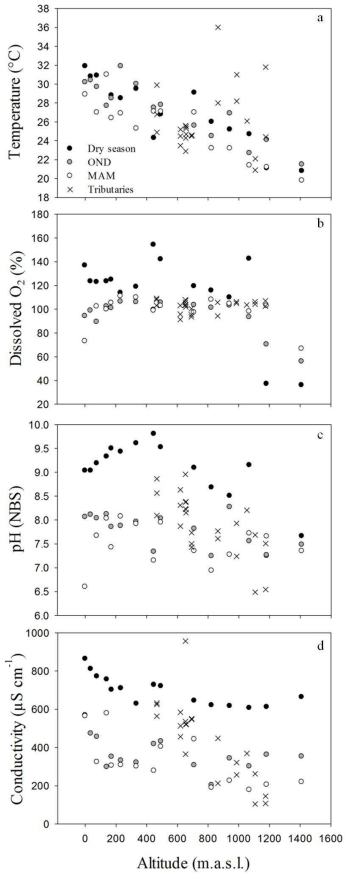

Fig. 2. Altitudinal gradient during dry season (August–September 2011), short rain season (October–December, OND, November 2011) and long rain season (March–May, MAM, April 2012) and tributaries (x, all seasons) of instream **(a)** temperature (°C), **(b)** dissolved oxygen (%), **(c)** pH (NBS), and **(d)** conductivity (µS cm^{-1}).

BGD
10, 8637–8683, 2013

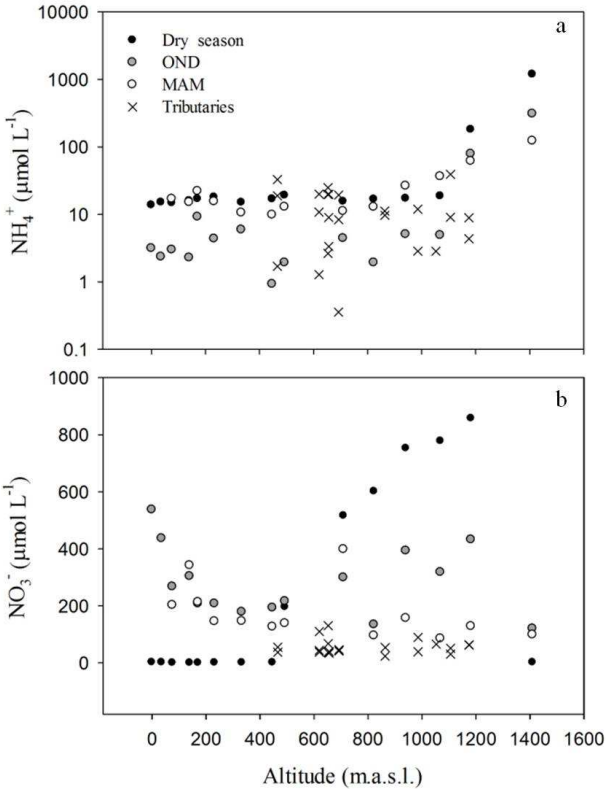

Fig. 3. Altitudinal gradient during dry season (August–September 2011), short rain season (October–December, OND, November 2011) and long rain season (March–May, MAM, April 2012) and tributaries (x, all seasons) of instream **(a)** NH_4^+ (µmol L^{-1}), and **(b)** NO_3^- (µmol L^{-1}). Note the logarithmic scale on the top panel.

BGD
10, 8637–8683, 2013

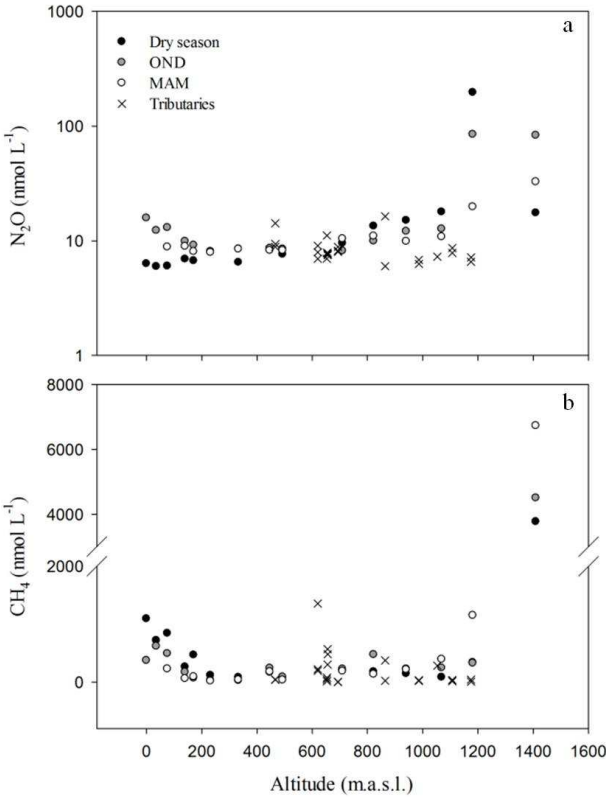

Fig. 4. Altitudinal gradient during dry season (August–September 2011), short rain season (October–December, OND, November 2011) and long rain season (March–May, MAM, April 2012) and tributaries (x, all seasons) of instream **(a)** dissolved N_2O (nmol L^{-1}), and **(b)** CH_4^- (nmol L^{-1}). Note the logarithmic scale on the top panel.

BGD
10, 8637–8683, 2013

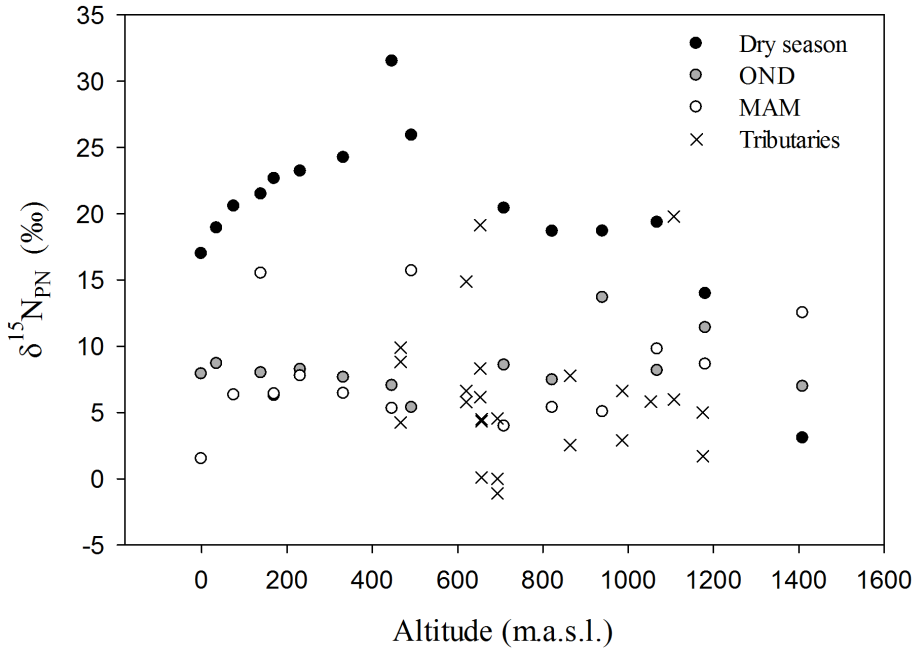

Fig. 5. Altitudinal gradient during dry season (August–September 2011), short rain season (October–December, OND, November 2011) and long rain season (March–May, MAM, April 2012) and all tributaries (x, all seasons) of instream $\delta^{15}N_{PN}$.

BGD
10, 8637–8683, 2013

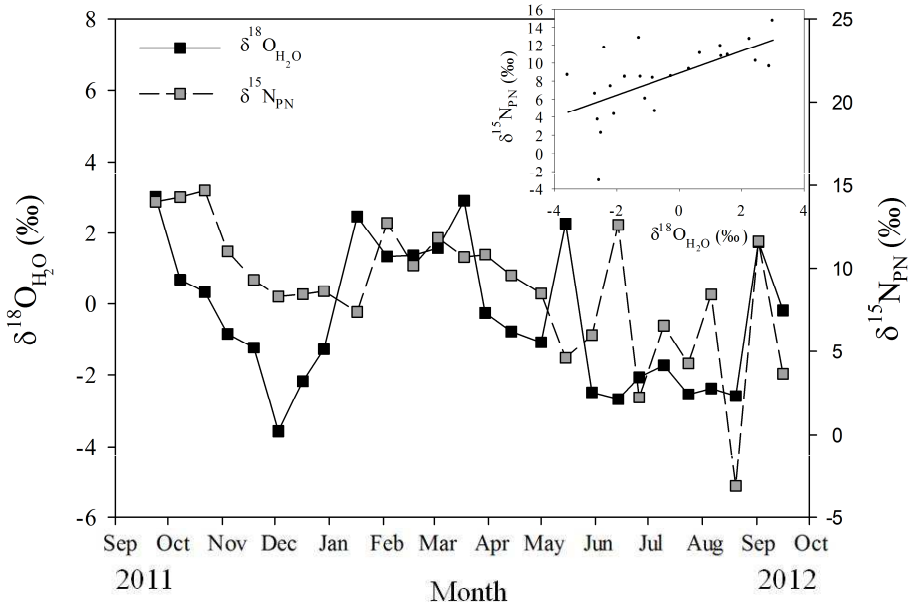

Fig. 6. A strong correlation was observed ($p = 0.0258$, $n = 26$) between $\delta^{18}O_{H_2O}$ and $\delta^{15}N_{PN}$ at S20 over a 12 month sampling period, with more enriched $\delta^{15}N_{PN}$ exported under drier conditions. (Inset) Linear regression of $\delta^{18}O_{H_2O}$ and $\delta^{15}N_{PN}$ with a one month forward shift of $\delta^{18}O_{H_2O}$ ($y = 8.8888 + 1.2241x$; $r^2 = 0.3878$). The relationship weakens without the forward shift of $\delta^{18}O_{H_2O}$ ($y = -2.2256 + 0.2098x$; $r^2 = 0.1905$).

BGD
10, 8637–8683, 2013

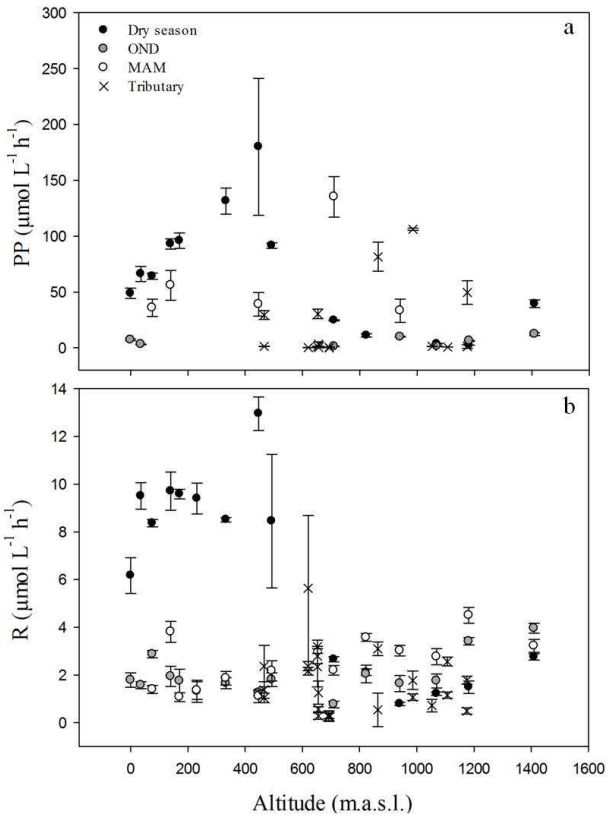

Fig. 7. Altitudinal gradient during dry season (August–September 2011), short rain season (October–December, OND, November 2011) and long rain season (March–May, MAM, April 2012) and tributaries (x, all seasons) of surface water **(a)** pelagic primary production (including error bars), and **(b)** community respiration rates (including error bars).

BGD
10, 8637–8683, 2013

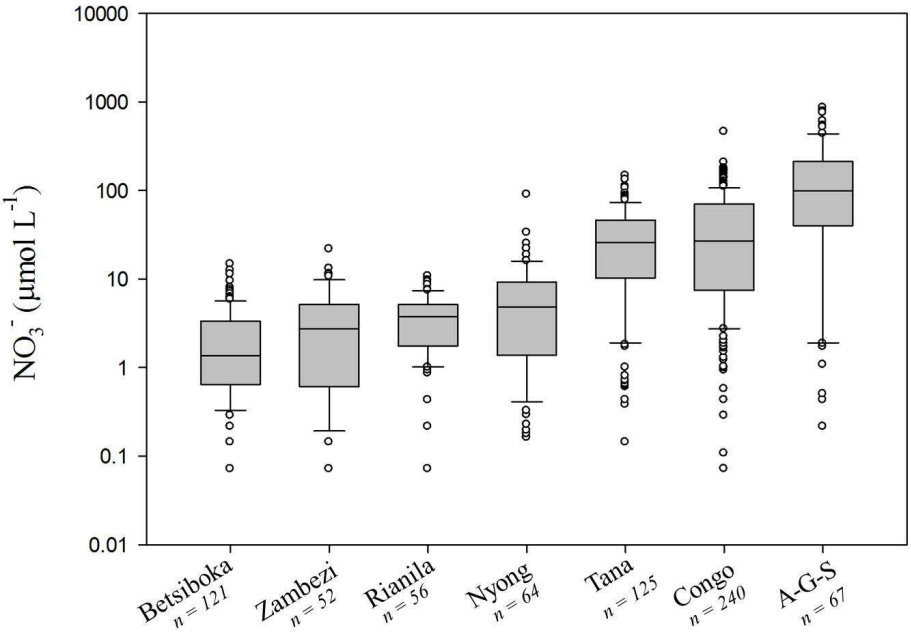

Fig. 8. Box plot of NO_3^- range for seven African river catchments. From left to right: Betsiboka catchment, Madagascar (own unpublished data); Zambezi catchment (own unpublished data); Rianila catchment, Madagascar (own unpublished data); Nyong catchment, Cameroon (Viers et al., 2000); Tana catchment, Kenya (Bouillon et al., 2009, and own unpublished data); Congo catchment (ORE-HYBAM and own unpublished data); and the Athi–Galana–Sabaki catchment, Kenya. Further data-sets included in text.

BGD
10, 8637–8683, 2013

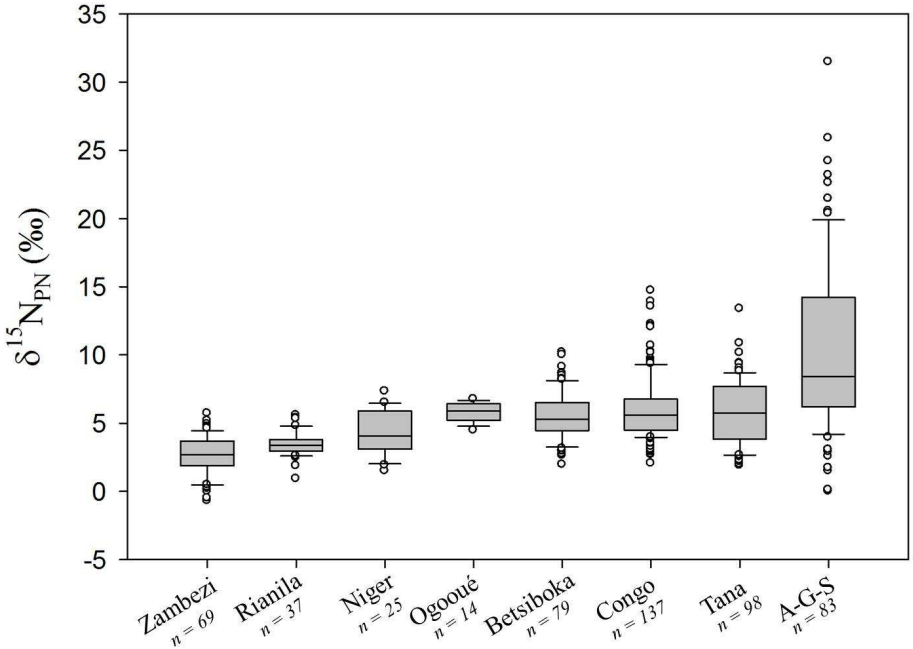

Fig. 9. Box plot of the range of $\delta^{15}N_{PN}$ data for eight African river catchments. From left to right: Zambezi catchment, Zambia and Mozambique (Zurbrügg et al., 2013 and own unpublished data); Rianila catchment, Madagascar (own unpublished data); Niger catchment, Niger (own unpublished data); Ogooué Catchment, Gabon (own unpublished data); Betsiboka catchment, Madagascar (own unpublished data); Congo catchment, Central African Republic and Democratic Republic of the Congo (own unpublished data); Tana catchment, Kenya (Bouillon et al., 2009, and own unpublished data); and the Athi–Galana–Sabaki catchment, Kenya.

BGD
10, 8637–8683, 2013

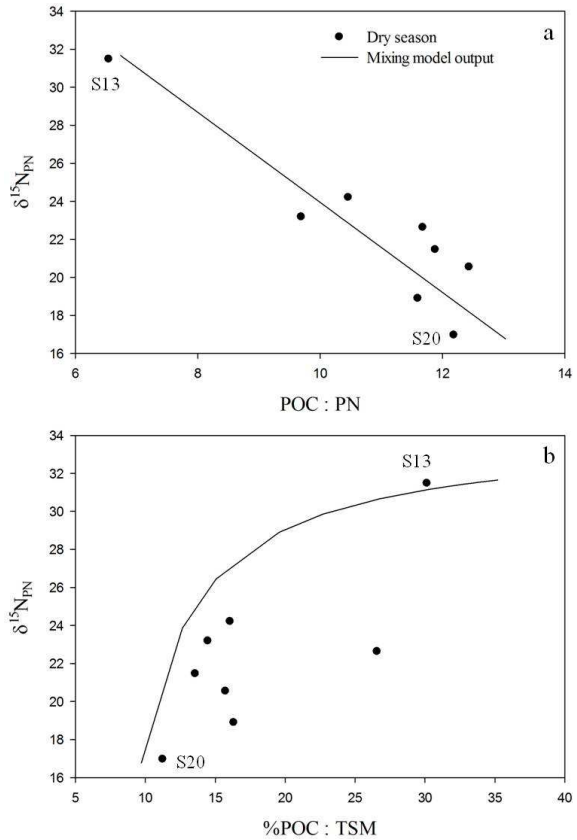

Fig. 10. Field measurements between S13 and S20 and mixing model output (solid line) for **(a)** POC : PN and $\delta^{15}N_{PN}$, showing the preferential metabolism of phytoplankton biomass and associated depletion of the $\delta^{15}N_{PN}$ pool downstream of the observed phytoplankton blooms. The non-linear relationship between **(b)** %POC : TSM and $\delta^{15}N_{PN}$ supports the suggestion of rapid removal of the labile phytoplankton biomass downstream of S13.

BGD
10, 8637–8683, 2013

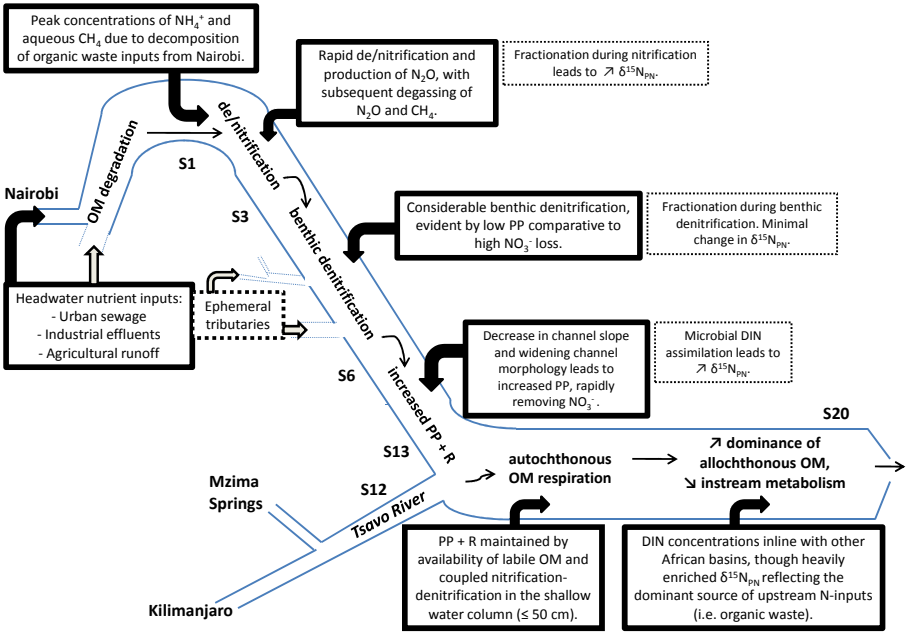

Fig. 11. Conceptual scheme of dry season N-cycling in the A–G–S river catchment, Kenya. (Upper left) Surface runoff and direct input of organic wastes in the upper catchment provide huge quantities of DIN at S1, much of which has been transformed and removed from the aquatic system below S13. Dominant processes and river characteristics along each reach (bold box with arrow) are outlined, as well as downstream evolution of the $\delta^{15}N_{PN}$ signature (dashed box).

BGD
10, 8637–8683, 2013